# Polarimetric Radar Observations of Hail Formation

Patrick C. Kennedy, Steven A. Rutledge, and Walter A. Petersen

*Department of Atmospheric Science, Colorado State University, Fort Collins, Colorado*

V. N. Bringi

*Department of Electrical Engineering, Colorado State University, Fort Collins, Colorado*

ABSTRACT

Analyses are made of the evolution of selected polarimetric radar data fields during periods immediately preceding the onset of near-surface hail indicators [high reflectivity and low differential reflectivity ($Z_{dr}$)] in two nonsupercellular northeastern Colorado hailstorms. The primary data were obtained from the 11-cm-wavelength, dual-polarization Colorado State University (CSU)–University of Chicago and Illinois State Water Survey radar. In one of the storms, dual-Doppler wind field syntheses were available using additional velocity data collected by the CSU Pawnee S-band radar. In both events, linear depolarization ratio (LDR) values exceeding $-25$ dB began to appear in the right flank of the 50-dBZ echo core region, within the $0°$ to $-20°$C environmental temperature range, approximately 10 minutes prior to the onset of hail at the surface. Scattering calculations suggest that the LDR enhancement may have been caused by an increasing water fraction within the growing hailstones (spongy hail), or the development of a liquid water coat under wet growth conditions. Vertical structure of the $Z_{dr}$ fields was also examined. As hypothesized by Conway and Zrnić, it was found that the distinctness of the positive $Z_{dr}$ column associated with supercooled raindrops and incompletely frozen particles above the $0°$C height varies from storm to storm.

## 1. Introduction

In general, the growth of hailstones is maximized when they collect appreciable quantities of supercooled cloud droplets, a condition most often attained in vigorous updrafts (Ludlam 1980). The resultant microwave radar backscatter properties are strongly affected by the evolution of hydrometeor size, concentration, phase, shape, and fall mode (Bringi et al. 1986b). Early observations of hailstorms were made using single-parameter radars. For example, Donaldson (1961) examined variations of radar reflectivity with height and found that echoes from storms generating large hail in New England typically penetrated the tropopause by about 1.5 km, but the echo summit of storms producing only small hail usually did not penetrate the tropopause. Over the last several decades, a variety of multiparameter radar observations of hailstorms have been made. (Here "multiparameter" implies radar observations made at more than one polarization and/or wavelength.) Atlas and Ludlam (1961) noted that appreciable reflectivity differences occurred when several radars operating on a variety of wavelengths scanned the same hailstorm. The reflectivity differences were attributed to the wavelength-dependent effects of Mie scattering. These observations suggested that the presence of hail could be inferred from a comparison of the reflectivities obtained through the simultaneous use of two different wavelengths. In principle, the reflectivities observed at the two wavelengths would become different when the presence of centimeter-sized hail made Mie resonance effects significant at the shorter wavelength. Several applications of the dual-wavelength hail detection method have been made (Heymsfield et al. 1980; Bringi et al. 1986b; Tuttle et al. 1989; Miller et al. 1990). However, the dual-wavelength method is very sensitive to antenna pattern matching at the two wavelengths (Rinehart and Tuttle 1982) as well as to attenuation effects at the shorter wavelength (Tuttle and Rinehart 1983).

To avoid the technological challenges posed by dual-wavelength methods, several polarimetric techniques (at a single wavelength) have been used to study hailstorms. Seliga and Bringi (1976, 1978) noted that inherent mean shape differences between freely falling hailstones and raindrops would have measurable microwave backscatter effects. To be specific, raindrops with diameters exceeding 1.5 mm assume oblate shapes with their major axes approximately horizontally oriented because of

*Corresponding author address:* Patrick C. Kennedy, Dept. of Atmospheric Science, Colorado State University, Fort Collins, CO 80523.
E-mail: pat@lab.chill.colostate.edu

combined gravitational, aerodynamic, and surface-tension effects (Pruppacher and Beard 1970). In contrast, hailstones are much more resistant to aerodynamic deformation and are more likely to tumble while falling (Knight and Knight 1970). Thus, the backscattering cross section of oblate raindrops will be greater at horizontal linear polarization (H) than at vertical linear polarization (V), whereas the H and V backscattering cross sections of hailstones will be more nearly equal. Seliga and Bringi (1976, 1978) proposed differential reflectivity $Z_{dr}$ as an expression of the H, V backscatter difference:

$$Z_{dr}(dB) = 10 \log_{10}(Z_{HH}/Z_{VV}), \qquad (1)$$

where $Z_{HH}$ is the copolar reflectivity at horizontal polarization and $Z_{VV}$ is the copolar reflectivity at vertical polarization.

Aydin et al. (1986) substantiated the utility of this technique by documenting ~0-dB S-band $Z_{dr}$ values in near-surface thunderstorm echo-core regions where the presence of hail was confirmed by ground observations. However, the raindrop–ice particle mean shape difference responsible for this $Z_{dr}$ hail signature generally disappears at subfreezing temperatures as the general presence of frozen scatterers quickly drives overall echo $Z_{dr}$ values toward 0 dB (Herzegh and Jameson 1992). An important departure from the preponderance of near-0-dB $Z_{dr}$ values in the subfreezing portions of convective echoes was noted by Illingworth et al. (1987). They documented several cases in which narrow (1–2 km in diameter), positive $Z_{dr}$ "columns" (4–6 dB) were found to extend briefly to heights of several kilometers above the 0°C level in isolated convective clouds that were developing in low–wind speed environments. They attributed this observation to the presence of large (>4 mm in diameter) supercooled raindrops that were lofted above the 0°C level by strong updrafts. Conway and Zrnić (1993) found the positive $Z_{dr}$ column to be a much longer-lived feature in a major Colorado hailstorm. In their case, the column was persistent during the ~40-minute quasi-steady-state period analyzed. The associated hail trajectory computations showed that significant hailstone growth typically occurred along trajectory segments that passed either through or immediately above the positive $Z_{dr}$ column.

None of these techniques made use of the depolarized component of the backscattered signal. Conceptually, depolarization is increased when the axes of symmetry of nonspherical particles are misaligned with the incident electric field vector (Atlas et al. 1953). For example, when the illuminating electric field is linearly polarized, the cross-polar return from an oblate particle is maximized when the particle's major diameter is oriented at a 45° angle to the incident electric field. These depolarization effects are magnified as the scatterer's water fraction increases, because of an increase in the bulk dielectric factor. Thus hailstones, particularly when they are experiencing wet or spongy growth conditions

(Lesins and List 1986), may induce appreciable depolarization levels because their shapes are typically nonspherical and their orientations often fluctuate significantly as they fall (Herzegh and Jameson 1992). Many of the original investigations of hail-related depolarization effects were carried out by Canadian researchers studying the interaction of circularly polarized radiation with various types of precipitation (McCormick and Hendry 1975). In circularly polarized radiation, the instantaneous polarization vector rotates with distance along the direction of propagation while maintaining fixed amplitude. The circular depolarization ratio (CDR) is defined by:

$$CDR(dB) = 10 \log_{10}(Z_{parallel}/Z_{orthogonal}), \qquad (2)$$

where $Z_{parallel}$ is the radar reflectivity based on the return signal with the same polarization sense as the transmitted pulse and $Z_{orthogonal}$ is the radar reflectivity based on the return signal with the opposite polarization sense as the transmitted pulse. For example, if left-handed circular is transmitted, $Z_{parallel}$ is the power return for LH circular and $Z_{orthogonal}$ is the power returned for RH circular. For spherical targets, CDR = $-\infty$. Increased CDR values measured with a 10-cm-wavelength radar (i.e., increased depolarization levels) were found to correlate with surface observations of hailstones larger than about 3 cm in diameter (Barge 1970). Enhanced CDR levels were also found in the elevated echo region overhanging a weak echo region (WER, Browning and Foote 1976), an echo area in which hail growth was likely. It was also found that when moderate to heavy rain rates were present along the beam path, differential propagation effects caused the incident circularly-polarized radiation to become elliptically polarized, complicating accurate CDR measurement (Humphries 1974).

Depolarization by hail has also been studied using linear polarization states. The linear depolarization ratio (LDR) is given by:

$$LDR(dB) = 10 \log_{10}(Z_{VH}/Z_{HH}), \qquad (3)$$

where $Z_{VH}$ is the cross-polar reflectivity: receive V and transmit H.

Bringi et al. (1986b) found that LDR observed at 3-cm wavelength was enhanced in the presence of hail. These LDR enhancements were also seen to extend vertically into the subfreezing cloud region above the locations where ~0-dB $Z_{dr}$ values indicated hail at ground level. As might be expected, the effects of attenuation on these X-band signals had to be carefully considered. However, the association between enhanced X-band LDR values at subfreezing temperatures and the presence of hail is not unambiguous. Smith et al. (1999) analyzed a region of >−21-dB X-band LDR values observed just above the top of a positive $Z_{dr}$ column in a Florida thunderstorm cell. In situ observations showed that the LDR enhancement was due raindrops in the process of freezing, not ice particles in wet growth. Holler et al. (1994) reported on 5-cm-wavelength radar
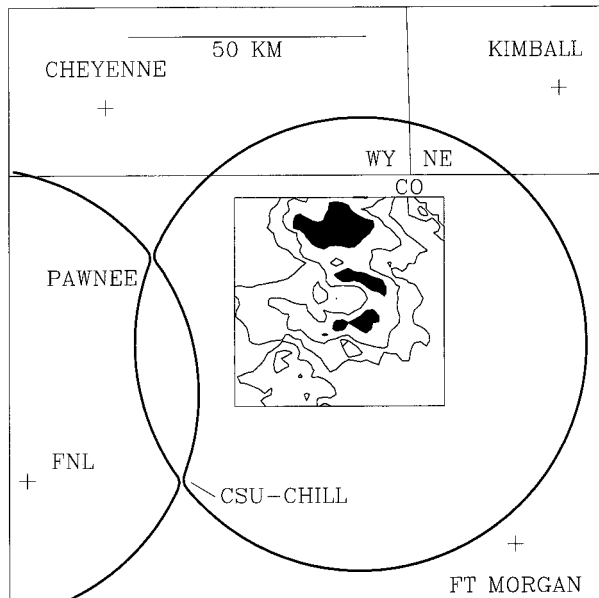
FIG. 1. The eastern lobe (>30° beam intersection angles) of the CSU–CHILL/Pawnee dual-Doppler network. CAPPI inset shows the 6-km-MSL reflectivity pattern at 2355 UTC 15 Jul 1998. Starting contour is 30 dBZ, contour interval is 10 dB, and areas within the 50-dBZ contour are filled.

observations made during the vigorous stage of a hybrid-type hailstorm in Germany. They found enhanced LDR values (>−25 dB) to be well-correlated with the existence of hail, particularly when the hail was experiencing wet growth conditions. Hubbert et al. (1998) analyzed the complete set of available polarimetric data in a supercell hailstorm in northeastern Colorado using the Colorado State University–University of Chicago and Illinois State Water Survey (CSU–CHILL) radar. They were able to relate a positive $Z_{dr}$ column and areas of enhanced LDR at midlevels to the production of large hail.

The goal of this study is to document the evolution of S-band LDR and $Z_{dr}$ patterns within the time period immediately preceding the onset of hail signatures at the lowest antenna elevation angle (interpreted as an indicator of surface hail). Observations are presented

from two hail-producing nonsupercell thunderstorms that took place over the high plains of Colorado. Once the low-elevation-angle hail signatures appeared, the polarimetric data indicated that both storms continued to deposit hail along 20–30-km swaths. During one of these storms, air motion fields could be synthesized from dual-Doppler measurements. Last some aspects of the observed evolution of LDR enhancement patterns are simulated through microwave scattering model calculations, as related to cloud microphysical processes.

## 2. Radar instrumentation and general data analysis procedures

The polarimetric radar data used in this study were collected by the S-band CSU–CHILL system located near Greeley, Colorado. The system's polarimetric measurement capabilities are enhanced through the use of a dual-transmitter–dual-receiver configuration (Brunkow et al. 2000). For all of the data described in this study, the dual transmitters were fired alternately, producing a steady H, V, H, V, . . . polarization sequence. The radar's dual receivers allow both the co- and cross-polar signal returns to be processed from each transmitted pulse. The LDR was computed according to Eq. (3).

During the summer of 1998, CSU also started operating the Pawnee Doppler radar, an 11-cm-wavelength, single-polarization Doppler radar located 48 km NNW of the CSU–CHILL site. This radar network permits dual-Doppler scanning to be maintained over portions of both the Front Range foothills and the adjacent high plains (Fig. 1). Summaries of each radar's performance characteristics are given in Table 1.

The analyzed cases were selected based upon the requirement that full three-dimensional echo scanning was in progress prior to the first observation of a hail signature at the lowest elevation angle. The radar scanning strategy varied among the two cases, affecting primarily the volume scan duration and elevation-angle step size. The hail signature was defined by the differential reflectivity hail signal (HDR) developed by Aydin et al. (1986). HDR is calculated by subtracting a prescribed function of $Z_{dr}$ from $Z_H$:

TABLE 1. Characteristics of the CSU–CHILL and CSU–Pawnee radar systems. SNR is signal-to-noise ratio.

|  | CHILL | Pawnee |
| --- | --- | --- |
| Wavelength (cm) | 11.009 | 10.989 |
| 3-dB beamwidth (°) | 1.0 | 1.6 |
| Peak transmit power (kW) | 800 | 380 |
| Pulse duration ($\mu$) | 1 | 1 |
| Pulse repetition frequency (Hz) | 1000 | 962 |
| Noise power (SNR = 1; dB$m$) | −114 | −109 |
| Polarization | H, V | V |
| Pulses per integration cycle | 128 (64 H + 64 V) | 128 |
| Lat (°N) | 40.446 | 40.871 |
| Long (°W) | 104.637 | 104.715 |
| Antenna elevation (m MSL) | 1432 | 1688 |

$$HDR = Z_H - f(Z_{dr}), \qquad (4)$$

where

$$f(Z_{dr}) = \begin{cases} 27 & \text{when } Z_{dr} \leq 0 \text{ dB} \\ 19Z_{dr} + 27 & \text{when } 0 < Z_{dr} \leq 1.74 \text{ dB} \\ 60 & \text{when } Z_{dr} > 1.74 \text{ dB}. \end{cases} \qquad (5)$$

The piecewise continuous $Z_{dr}$ function given by Eq. (2) was based on disdrometer measurements and represents the limiting $Z_{dr}$ values that were realized in pure rain with varying reflectivity levels. Thus, positive HDR values signify a situation in which the observed $Z_{dr}$ is appreciably below that expected from pure rain with the same reflectivity. Aydin et al. (1986) found good correlation between HDR values and observations of surface hail in Colorado thunderstorms. In this study, the onset of surface hail was taken to be the first appearance of HDR values exceeding 5 dB in the lowest sweep (nominally, the 0.5° elevation sweep).

Once the radar-determined hail onset time was identified, data from the preceding volumes were examined in detail. Considerable efforts were made to eliminate artifacts from the radar data. The data were interactively edited using the National Center for Atmospheric Research's Research Data Support System software (Oye and Carbone 1981). Conventional methods of applying thresholds were used to remove noise effects, and velocities were interactively dealiased. Polarimetric radar data were excluded when the correlation at zero time lag between the H and V return signals ($\rho_{hv}(0)$ Balakrishnan and Zrnić 1990) fell below 0.80–0.85. To avoid corruption from low signal-to-noise ratios, LDR values were only used when the signal plus noise power in the cross-polar channel was at least 2 dB above the associated receiver noise level. Last, to limit artifacts introduced by mismatches between the antenna H and V radiation patterns, both the $Z_{dr}$ and LDR range gate values were deleted from areas where either the azimuth plane or elevation plane spatial reflectivity gradients (cross-beam gradients) exceeded a range-dependent threshold of approximately 23 dB km$^{-1}$ (Brunkow et al. 2000).

It was necessary to determine LDR values that indicated a significant degree of depolarization, particularly in subfreezing echo areas. Mie scattering effects materially increase the return signal depolarization; thus the large LDRs (exceeding −16 dB) observed at X band by Bringi et al. (1986b) in an intense hailstorm are not expected at S band. Numerous histograms generated from CSU–CHILL data at subfreezing temperature levels showed that the average LDR levels were generally about −28 to −26 dB in most convective echo regimes (typical of medium density graupel, Holler et al. 1994). LDRs often increased to values greater than −25 dB near the echo summit, perhaps due to an increasing fraction of higher-density, less spherically shaped, anvil-level ice particles. In this work, LDR ≥ −25 dB was taken to indicate the presence of hail in regions associated with subfreezing temperatures and within the "active" (nonanvil) portions of a convective storm echo.

## 3. Radar observations

### a. 15 July 1998

During the predawn hours of 15 July 1998 a weak upslope wind pattern had developed at the surface and increased the low-level moisture content. By 1925 UTC the dewpoint temperature at Greeley had reached 10.6°C. Based on the 1200 UTC Denver (DNR) sounding modified to reflect the late-afternoon environment, the lifting condensation level (LCL) was estimated to be at a pressure of 590 hPa and a temperature of +4.7°C, with a mixing ratio of ~8.7 g kg$^{-1}$. (No DNR sounding data were available for 0000 UTC 16 July 1998.) Widely scattered thunderstorms that developed over the Rocky Mountain foothills moved eastward past the CSU–CHILL radar during the late-afternoon hours. Between 2345 UTC 15 July and 0030 UTC 16 July, these storms organized into a short north–south-oriented line located within the eastern lobe of the CSU dual-Doppler network (Fig. 1). (All time references are in UTC; local time is UTC minus 6 h.) The echo from the storm of interest began to develop rapidly around 2340 and by 0015 had become a major element in the evolving convective line. HDR values (Aydin et. al. 1986) were computed for each gate in the 0.5° elevation-angle data. An expanding area of positive (>5 dB) HDR values was first observed in the 0004 data; therefore this was taken to be the time that hail started to arrive at the surface (Figs. 2a,b). Because of extremely low population densities, surface observations related to this HDR feature were not available. The nearest available hail report was 25-mm (1 in.)–diameter stones reported near $X = 47$, $Y = 51$ km from the CSU–CHILL radar at 0025 UTC. This point was in the path of the northernmost echo core shown in Fig. 1.

Dual-Doppler air motion analyses were carried out for the three volume scans immediately preceding the appearance of the 0.5° elevation-angle HDR hail indicator. In each of these dual-Doppler analyses, a Cressman (Cressman 1959) weighting scheme was used to interpolate the edited data from the CSU–CHILL and Pawnee radars to a common Cartesian grid. Grid heights were referenced to sea level. The grid spacing was 1 km in $X$ and $Y$ and 0.75 km in $Z$; the radius of influence was 0.5 km. Horizontal wind field synthesis based on the gridded radial velocities was done via the Custom Editing and Display of Reduced Information in Cartesian Space software package (Mohr and Miller 1983). A correction for echo advection based on the radar-observed storm motion was applied during the syntheses, producing analyses valid at 2349, 2355, and 2359. The three synthesized airflow components were itera-
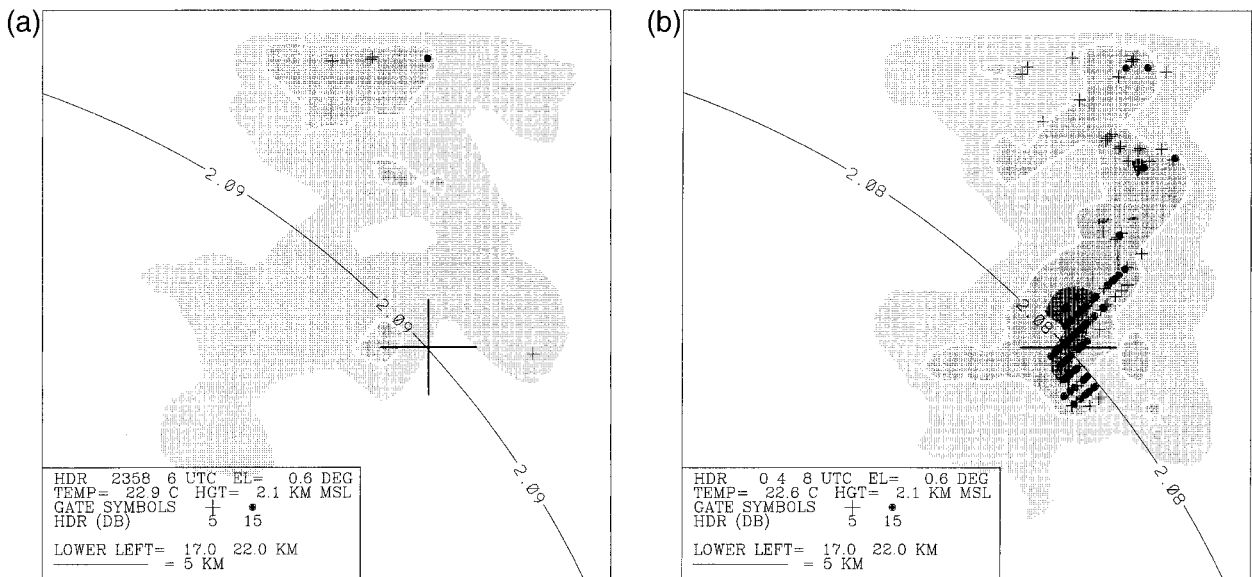
FIG. 2. (a) Shaded contours of reflectivity values (40, 50, and 60 dBZ) at 0.6° elevation angle for 2358 UTC 15 Jul 1998. Labeled arc is a constant-height line (km MSL) on the PPI scan surface. Terrain height is ~1.4 km MSL. Plotted symbols depict individual range gate HDR values (dB), where a plus indicates HDR > 5 dB and a dot indicates HDR > 15 dB. See text for explanation of HDR. Large "+" indicates approximate center of the HDR hail signature at 0004 UTC. (b) As in (a), except data were obtained at 0004 UTC 16 Jul 1998.

tively adjusted to account for the effects of vertical motions on the horizontal winds obtained from the dual-Doppler equations. Divergence fields were calculated from the adjusted horizontal winds at each analysis height. Vertical airflow was obtained by vertically integrating these horizontal divergence fields. The integration procedure imposed a variational constraint that forced the vertical velocities to 0 m s$^{-1}$ at the endpoints of the integration paths.

In the 2349 analysis, the storm cell of interest was intensifying aloft. At 6 km (about $-12$°C environmental temperature), this development was taking place within the curved 30-dBZ echo appendage that extended approximately 20 km SSE from a preexisting storm (Fig. 3). The reference lines in this figure that cross $X = 37.4$, $Y = 34.2$ km show the location where the 0.5° elevation-angle HDR hail signature will appear at 0004. Moderate southerly storm relative airflow was found over the future hail reference site. Stronger southeasterly inflow was located ~10 km further west ($X = 27$, $Y = 33$ km). A small region of positive ($>1$ dB) $Z_{dr}$ values was located approximately 3 km southwest of the reference point ($X = 34$, $Y = 32$ km). At two grid points within this region, $Z_{dr}$ exceeded $+1.5$ dB. The majority of the positive $Z_{dr}$ values at 6 km were located 10–15 km further north in the inflow to the preexisting storm. No areas of significant ($>-25$ dB) LDR values were found in the vicinity of the impending hail location at this time.

Significant differences were evident in the next volume scan (6 minutes later; 2355 analysis time). A regional increase in reflectivities had taken place, resulting in the formation of a contiguous, U-shaped 40-dBZ echo

area that enveloped the reference point (Fig. 4). This area contained several maxima exceeding 50 dBZ, one of which was located above the 0004 hail signature area. Horizontal winds in the intensifying echo backed towards the southeast and strengthened as the confluence axis approached. Updraft strength had also increased appreciably, with a maximum of greater than 20 m s$^{-1}$ extending south-southwestward from the reference mark. Within and immediately downstream of this updraft, an expanding area of positive $Z_{dr}$ values had developed (Fig. 4; $X = 34$, $Y = 34$ km). Peak grid point $Z_{dr}$ values of 3 dB were found ~2 km west of the reference mark. Conway and Zrnić (1993) noted a similar horizontal displacement between the axes of the positive $Z_{dr}$ column and the updraft maximum. Significant depolarization ($>-25$ dB), as represented by red color-coded horizontal wind vectors in Fig. 4 (see caption for details), had appeared in a contiguous north–south-oriented region that included the 50-dBZ echo cores within the 40-dBZ U-shaped echo.

The third consecutive volume (2359) was the last one in which no HDR hail signature was present in the 0.5° elevation-angle plan position indicator (PPI) data. The 6-km reflectivity pattern continued to intensify and organize (Fig. 5). A north–south-oriented band of reflectivities of greater than 50 dBZ had developed, with embedded maxima now exceeding 60 dBZ. By this time, the horizontal confluence zone had moved eastward to a position within 2 km of the impending surface hail signature location at 0004. Updrafts > 15 m s$^{-1}$ were located a few km east of the confluence axis. However, the areal coverage of updrafts > 20 m s$^{-1}$ had decreased somewhat near the reference mark. An area of distinc-
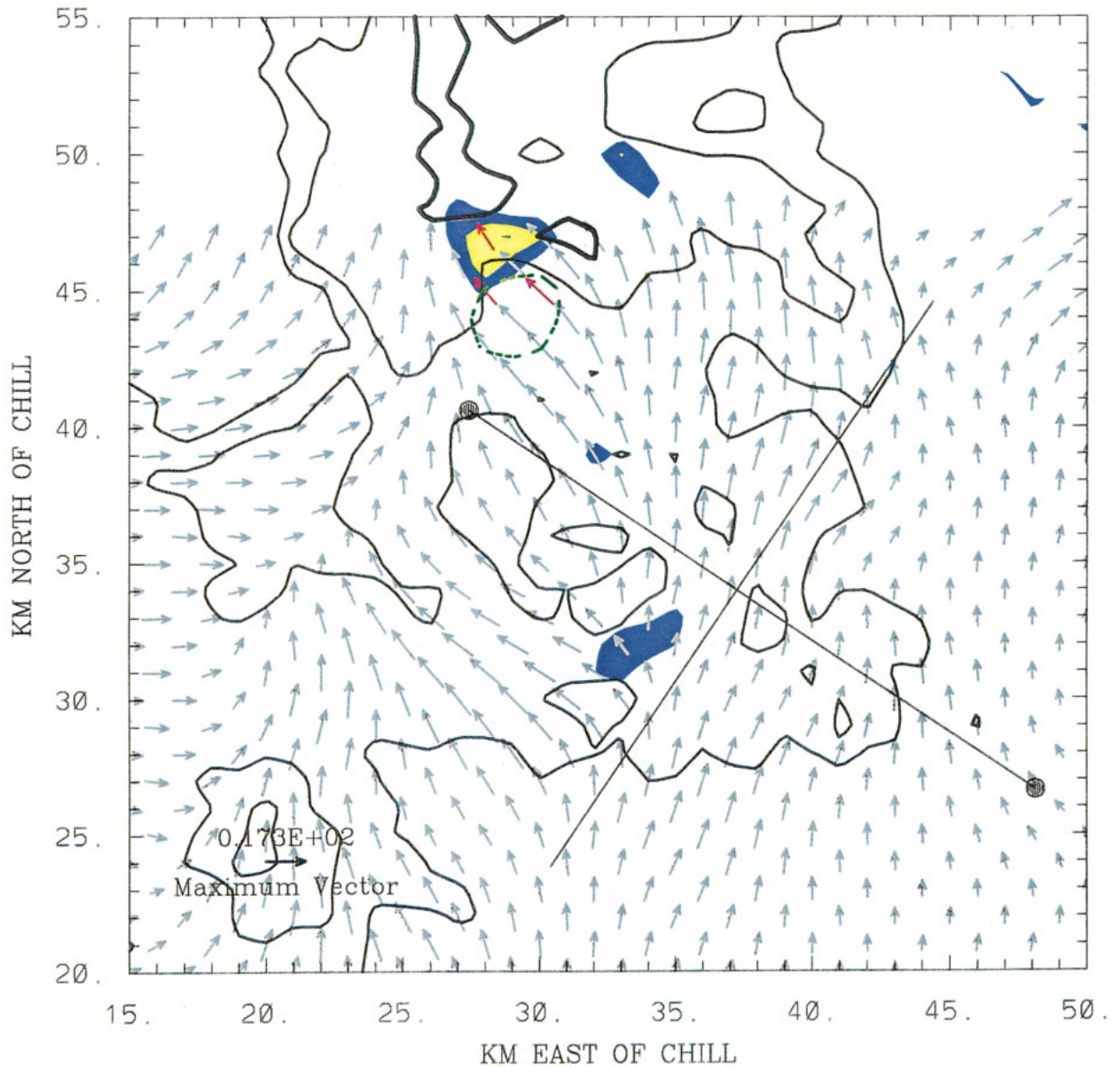
FIG. 3. Dual-Doppler analysis at 2349 UTC 15 Jul 1998. Analysis height is 6 km MSL, black contours are CSU–CHILL reflectivity levels (dBZ). The 50-dBZ contour is darkened. Vectors are storm-relative horizontal winds, the vector length scale is in the lower-left corner of the plot. Wind vector color codes depict gridpoint LDR values: gray = $< -25$ dB, red = $-25$ to $-22$ dB, and black = $> -22$ dB. (Black vectors do not appear until next analysis time; Fig. 4.) The $Z_{dr}$ levels are color shaded; starting shade is 1.0 dB, and interval is 1.0 dB. Green broken contours are updraft velocities; starting contour is 15 m s$^{-1}$, and interval is 5 m s$^{-1}$. Location of vertical cross section is depicted by line whose ends are marked with large dots. Perpendicular line intersects the cross section within the 0004 UTC HDR hail signature area.

tively positive $Z_{dr}$ values [at 6 km above ground level (AGL)] extended southward from the incipient HDR hail location. The axis of enhanced LDR had similarly advected eastward so as to become centered over the reference mark. Furthermore, much of the $> -25$-dB LDR area was now associated with reflectivities exceeding 50 dBZ.

A complementary view of the evolution of the radar data fields prior to the onset of surface hail is provided

by a series of vertical cross sections extracted from the three dual-Doppler analyses. These cross sections were all constructed on a gridpoint network that was rotated into alignment with the mean echo motion (from 304° at 8.2 m s$^{-1}$). The vertical cross section's location is shown by the cross-hair line whose ends are highlighted with solid dots in Figs. 3–5.

The cross section from the 2349 analysis showed an elevated echo maximum of between 40 and 50 dBZ over
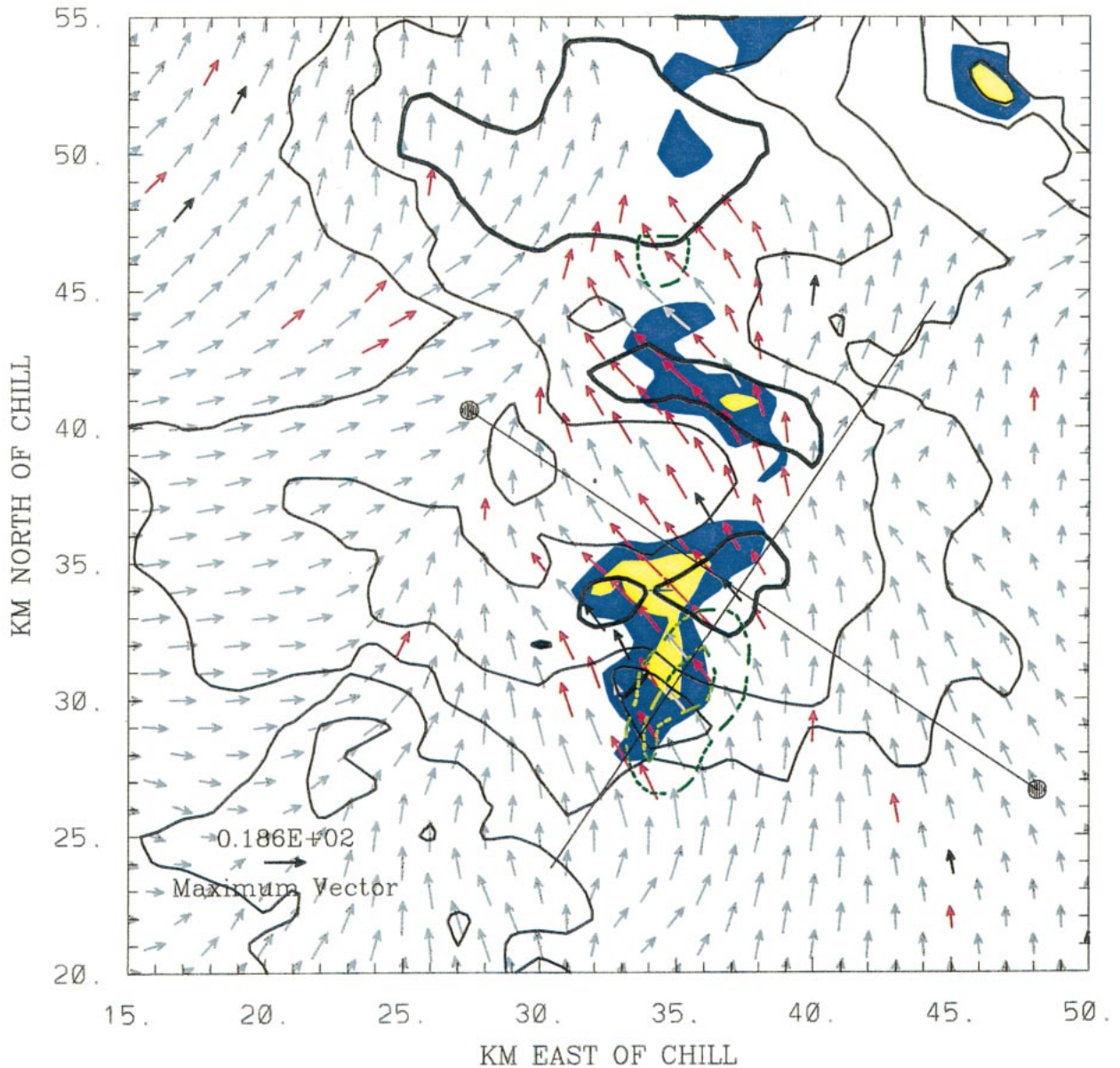
FIG. 4. As in Fig. 3, except analysis time is 2355 UTC.

the 0004 UTC hail signature site (Fig. 6). Above a point 1–2 km west-northwest of this future hail signature site, positive $Z_{dr}$s greater than 1.0 dB extended approximately 1 km above the 0°C height level. There were no indications of $>-25$-dB LDR values.

As noted in the 6-km constant-altitude PPI (CAPPI) discussion, obvious echo development was under way during the next volume scan. In the 2355 analysis an expanding area of $>50$-dBZ echo had appeared at midlevels above $Y = -10$ to $-13$ km (Fig. 7). This intensifying elevated echo mass was closely associated with the strongest (15–20 m s$^{-1}$) midlevel updrafts. In concert with the strengthening updraft, $Z_{dr}$ values in the column had increased significantly, with values of great-

er than 1 dB reaching a height of 6.75 km at $X = -10$ km. An elevated region of LDRs exceeding $-25$ dB had appeared that overlapped and surmounted the top of the positive $Z_{dr}$ column. This LDR signature was correlated well with the region where the 50-dBZ reflectivity contour was expanding aloft. A separate area of enhanced LDRs had appeared just below the 0°C height in the inflow region ($X = -16$, $Z = 3.75$–4.5 km). Melting of precipitation particles falling from the overlying echo mass into the storm inflow could have caused this LDR increase.

The positioning of the developing enhanced LDR area immediately above the summit of the positive $Z_{dr}$ column in the 2355 vertical cross section is notable. This
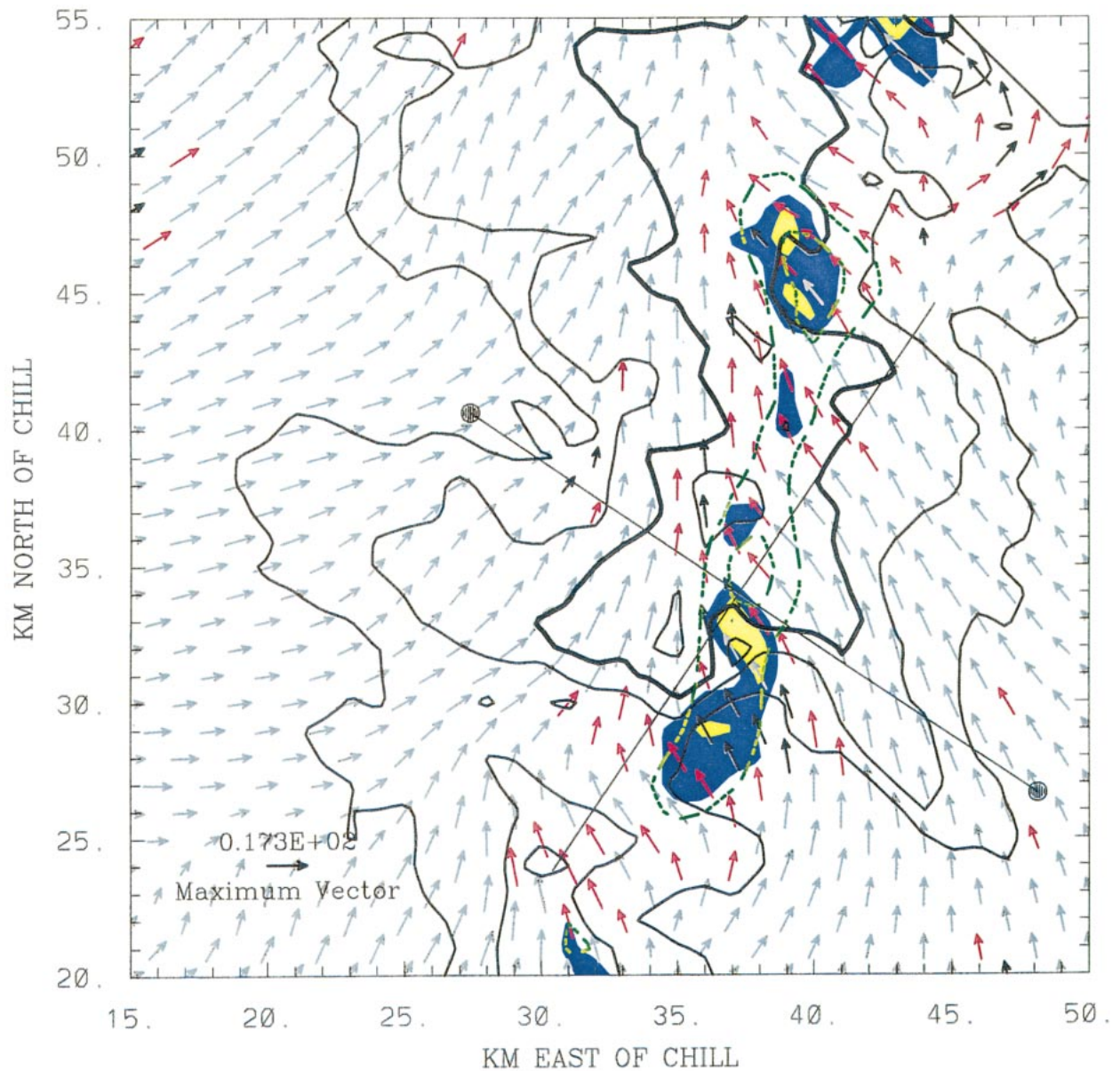
FIG. 5. As in Fig. 3, except analysis time is 2359 UTC.

arrangement suggests that the large supercooled rain-drops responsible for the positive $Z_{dr}$ column began to freeze as the updraft carried them into a progressively colder environment (Smith et al. 1999). As these particles froze, they were more likely to tumble (Spengler and Gokhale 1972), thus producing larger LDR values (Jameson et al. 1996). These newly-frozen particles were still exposed to the moisture flux provided by the updraft; an environment in which they could continue to grow rapidly by accretion (Johnson 1987). Thus, the 2355 analysis captured a time when the polarimetric radar signatures indicated that hail was growing aloft but had not yet reached the surface in appreciable quantities. The presence of the positive $Z_{dr}$ column in this

case suggests that freezing of millimeter-sized drops provided an immediate source of hail embryos.

In the third successive dual-Doppler analysis (2359), noticeable vertical expansion of the 50-dBZ reflectivity region had occurred, with 50-dBZ echo extending from 2.25 km above mean sea level (MSL; ~0.9 km AGL) to 12 km MSL (Fig. 8). A WER was suggested by the localized upward displacement of the 50-dBZ contour above $Y = -12$ km. The positive $Z_{dr}$ column persisted while becoming slightly shorter and narrower. The base of the significant LDR area descended to at least as low as 3 km MSL on either side of the 50-dBZ contour on the leading edge of the intense precipitation shaft. This is very close to the location where the HDR hail sig-
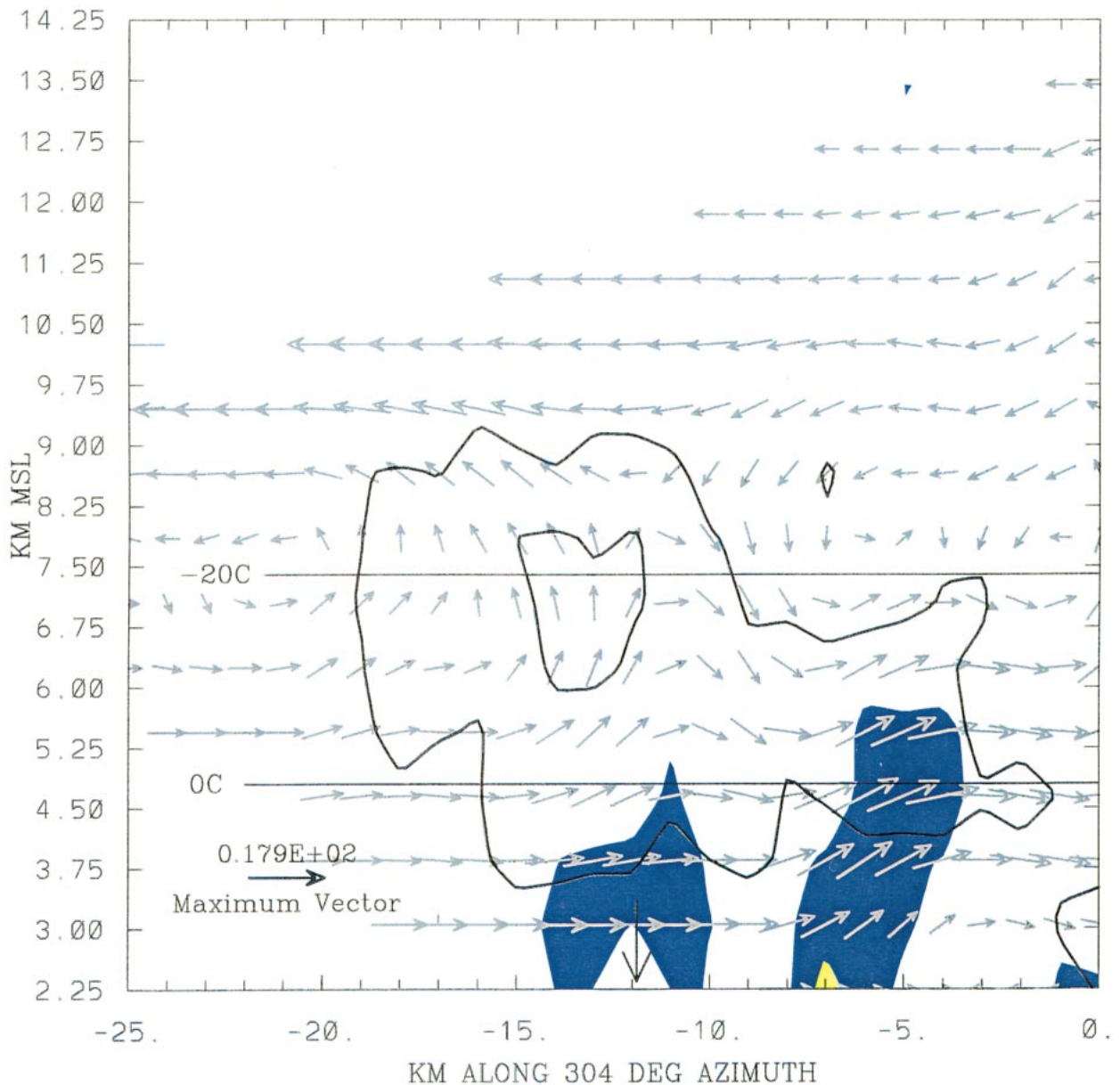
FIG. 6. Vertical cross section along the 304° azimuth at 2349 UTC 15 Jul 1998. Cross-section location is shown by the line with solid circle endpoints in Fig. 3. Contours are CSU–CHILL reflectivity levels at 10-dB intervals from a starting value of 30 dBZ. The $Z_{dr}$s are color shaded starting at 1.0 dB, with an interval of 1.0 dB. Wind vector horizontal components are storm relative; speed calibration vector is in the lower-left corner of the plot. Wind vector color codes depict gridpoint LDR values: gray = $< -25$ dB, red = $-25$ to $-22$ dB, and black = $> -22$ dB. (At 2349 UTC, no LDRs exceed $-25$ dB in the plot plane. The multicolored wind vectors will appear in Fig. 7.) The downward-pointing arrow near $-12$ km on the horizontal axis marks the 0004 UTC HDR hail signature location.

nature appeared in the next 0.5° PPI sweep (0004 UTC). Appreciable upward expansion of the $-25$-dB LDR contour had also taken place. However, at heights above ~9 km MSL, the enhanced LDR areas tended to be found in regions of less-than-50-dBZ reflectivity levels. The "crown" of significant LDR values found in the vicinity of the main updraft at heights above ~10 km MSL is probably due to heavily rimed, irregularly shaped graupel particles that were carried up into the anvil. Particles reaching these heights probably exited

the storm in the anvil outflow and thus did not participate in the hail formation process (Miller et al. 1990).

A more detailed analysis of the LDR evolution was made by examining CSU–CHILL individual range gate data in the three volume scans presented above. Specifically, regions in which the reflectivity from the storm of interest exceeded 40 dBZ in each PPI sweep were identified. Within these echo regions, counts of the number of range gates with LDR values greater than or equal to $-25$ dB were made for each PPI sweep.
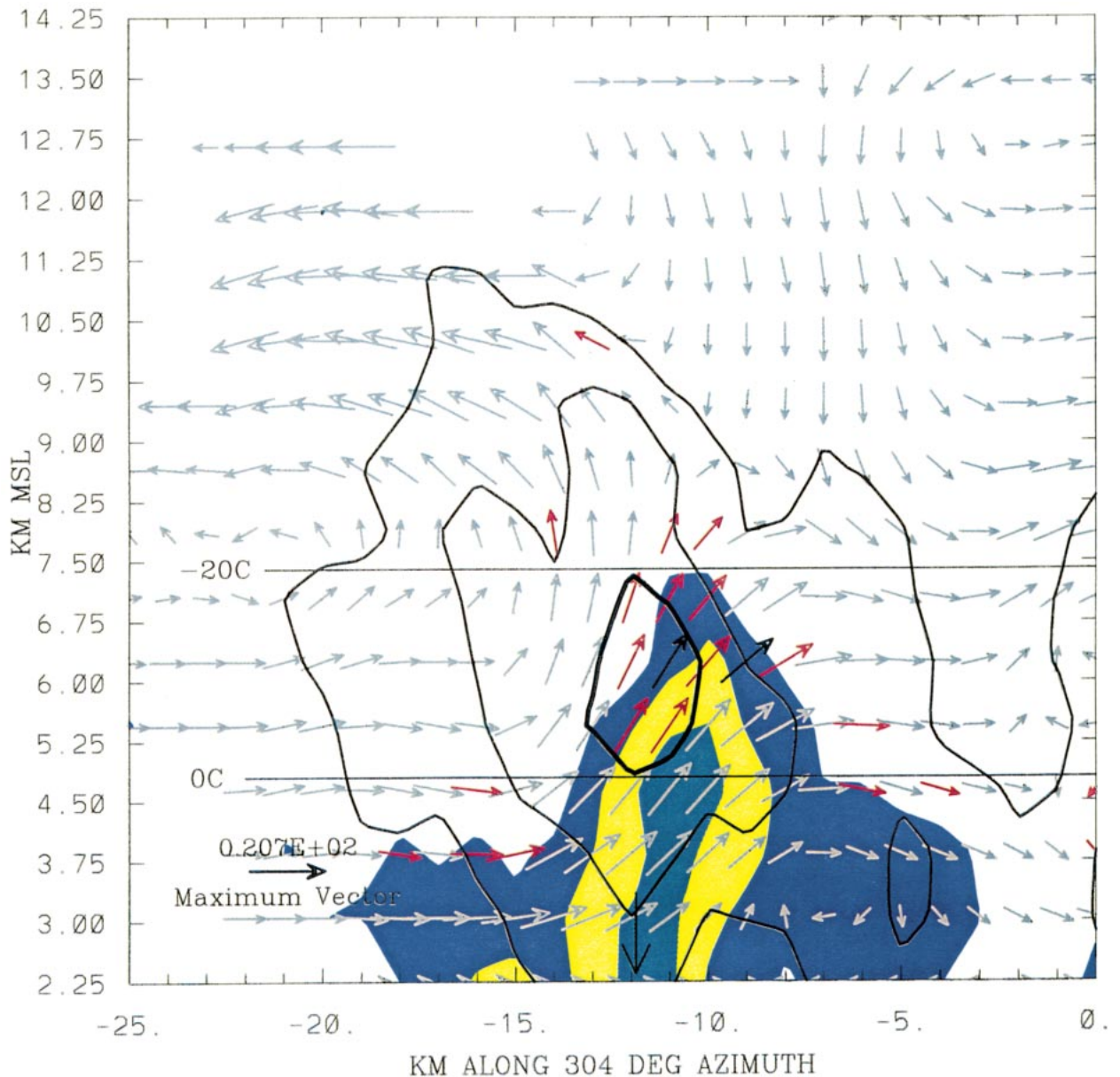
FIG. 7. As in Fig. 6, except analysis time is 2355 UTC.

A summary of this sweep-by sweep tabulation of echo-core range gates containing significantly large LDR values is shown in Table 2. The table values show the consistent trend for an increasing number of gates containing LDRs $> -25$ dB to appear in the 0 to $-20°C$ height band prior to the onset of an HDR hail signature on sweep 1. Furthermore, the percentage of the significantly depolarized gates that are associated with reflectivities of greater than 50 dBZ (i.e., column 5 of Table 2) also shows an increasing trend with time. Last, note that some significant LDR gates were detected in the above-freezing portions of the echo in all three of these volumes. These are thought to be due to small, melting ice or hail particles. Because $Z_{dr}$ is sensitive to

the scatterer's reflectivity-weighted mean aspect ratio (Jameson 1983), the HDR hail signature (a low-$Z_{dr}$ region within a high-reflectivity echo core) does not appear until hailstones become an appreciable fraction of the larger-diameter end of the precipitation particle size spectrum.

Taken together, the analyses of the 15 July 1998 case imply that significant hail growth was closely connected with an updraft that increased from $<10$ to $>20$ m s$^{-1}$ at midlevels between 2346 and 2352 UTC. A positive $Z_{dr}$ column associated with this strengthening updraft became increasingly apparent. A region of significant depolarization and rapidly intensifying reflectivity developed immediately above (and probably downwind
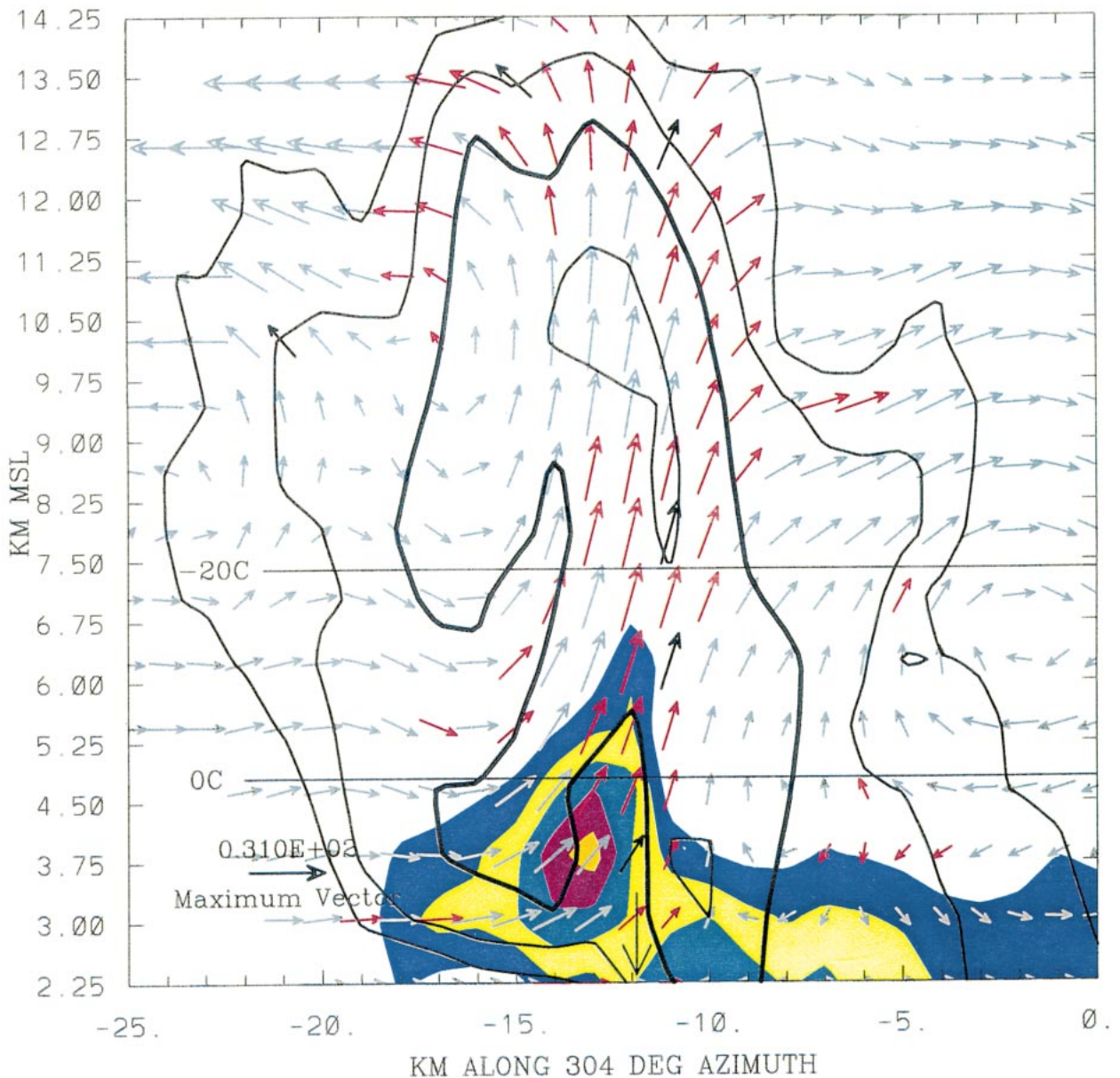
FIG. 8. As in Fig. 7, except analysis time is 2359 UTC.

from, in a relative sense) the summit of the $Z_{dr}$ column. Within the >50-dBZ portion of this elevated echo core, an appreciable fraction (>~40%–50%) of the range gates contained significant LDR values. The HDR hail signature appeared at the 0.5° elevation angle as the echo core with significant depolarization descended to the surface. Additional evidence for this evolutionary pattern will next be sought in a second hail event.

### b. 28 July 1996

The storm of interest on this date was a long-lived multicell that periodically generated large hail as it tracked southeastward from Wyoming toward the CSU–CHILL radar. Based on the 28 July 00 UTC DNR sounding, conditions at the LCL (~620 hPa) were estimated to be the following: temperature $T = +4.7°C$ and a saturation mixing ratio of ~8.7 g m$^{-3}$. These quantities were very similar to those for the 15 July 1998 case. The hail episode under analysis first presented a definitive HDR hail signature in the 0.5° elevation-angle PPI data at 2205. Note also that, between 2230 and 2250, this same storm produced significant damage resulting from 7-cm (2.75 in.)-diameter hail that fell near the town of Galeton, Colorado (NCDC 1996, 35–37).

The PPI-sector volume scan data collected by the CSU–CHILL radar on 28 July 1996 were interpolated to a Cartesian gridpoint network using the same methods

TABLE 2. 15 Jul 1998 sweep-by-sweep counts of gates exceeding selected LDR values.

| LDR categories (dB) | | | | Percent of LDR > −25 dB within 50-dBZ echo | Avg height (km MSL) | Estimated moist adiabatic temperature (°C) | Avg sounding temperature (°C) |
|---|---|---|---|---|---|---|---|
| −19 | −21 | −23 | −25 | | | | |
| 2346:04 UTC volume | | | | | | | |
| 0 | 0 | 2 | 6 | 0 | 9.5 | −27.2 | −31.7 |
| 0 | 0 | 19 | 22 | 2 | 9.7 | −28.3 | −33.1 |
| 0 | 1 | 6 | 50 | 9 | 9.3 | −25.2 | −30.4 |
| 0 | 4 | 9 | 26 | 15 | 8.8 | −22.0 | −27.0 |
| 0 | 0 | 1 | 22 | 4 | 8.3 | −18.5 | −23.6 |
| 0 | 0 | 0 | 20 | 40 | 7.8 | −14.8 | −21.3 |
| 0 | 2 | 8 | 53 | 22 | 7.4 | −11.7 | −20.0 |
| 0 | 12 | 18 | 37 | 16 | 6.8 | −8.1 | −16.4 |
| 2 | 15 | 33 | 68 | 36 | 6.1 | −3.8 | −11.1 |
| 1 | 11 | 46 | 105 | 17 | 5.3 | 0.8 | −4.3 |
| 0 | 12 | 43 | 211 | 4 | 4.6 | 3.7 | 1.8 |
| 0 | 4 | 40 | 190 | 6 | 3.9 | 8.7 | 8.5 |
| 0 | 5 | 30 | 88 | 18 | 3.2 | 16.3 | 15.2 |
| 0 | 0 | 2 | 34 | 14 | 2.6 | 21.7 | 19.2 |
| 0 | 14 | 39 | 58 | 15 | 2.0 | 27.0 | 23.3 |
| 2352:06 UTC volume | | | | | | | |
| 0 | 0 | 0 | 2 | 0 | 12.4 | −50.4 | −50.2 |
| 0 | 0 | 0 | 1 | 0 | 11.8 | −45.9 | −46.6 |
| 0 | 0 | 4 | 42 | 2 | 11.2 | −41.3 | −42.9 |
| 1 | 4 | 5 | 11 | 0 | 10.7 | −36.7 | −39.8 |
| 0 | 0 | 10 | 33 | 5 | 10.3 | −33.4 | −37.1 |
| 0 | 0 | 13 | 46 | 2 | 9.9 | −30.5 | −34.4 |
| 0 | 2 | 15 | 51 | 1 | 9.5 | −27.1 | −31.7 |
| 2 | 4 | 13 | 65 | 9 | 9.1 | −23.7 | −29.0 |
| 3 | 3 | 19 | 87 | 13 | 8.6 | −20.5 | −25.6 |
| 2 | 16 | 33 | 98 | 35 | 8.0 | −16.3 | −22.0 |
| 14 | 43 | 65 | 119 | 38 | 7.4 | −11.8 | −20.0 |
| 8 | 64 | 67 | 181 | 34 | 6.8 | −8.1 | −16.4 |
| 13 | 71 | 176 | 262 | 37 | 6.2 | −4.2 | −12.0 |
| 6 | 29 | 168 | 352 | 33 | 5.4 | −0.2 | −5.3 |
| 0 | 22 | 159 | 360 | 16 | 4.6 | 3.6 | 1.8 |
| 2 | 8 | 117 | 403 | 10 | 3.9 | 8.0 | 8.5 |
| 1 | 17 | 79 | 280 | 11 | 3.3 | 15.7 | 14.2 |
| 0 | 7 | 25 | 95 | 17 | 2.6 | 21.5 | 19.2 |
| 3 | 14 | 50 | 105 | 12 | 2.0 | 26.9 | 23.3 |
| 2358:06 UTC volume | | | | | | | |
| 0 | 0 | 0 | 0 | 0 | 14.5 | −60.0 | −59.9 |
| 0 | 0 | 0 | 0 | 0 | 13.5 | −55.1 | −55.3 |
| 0 | 1 | 3 | 17 | 0 | 12.6 | −51.0 | −51.1 |
| 0 | 2 | 21 | 91 | 2 | 11.8 | −45.5 | −46.6 |
| 0 | 10 | 43 | 112 | 13 | 11.1 | −40.5 | −42.3 |
| 1 | 4 | 52 | 117 | 33 | 10.4 | −34.8 | −37.8 |
| 0 | 9 | 60 | 110 | 35 | 9.9 | −30.0 | −34.4 |
| 3 | 36 | 107 | 168 | 26 | 9.5 | −26.7 | −31.7 |
| 6 | 57 | 156 | 220 | 23 | 9.2 | −24.6 | −29.7 |
| 0 | 79 | 207 | 378 | 32 | 8.8 | −22.1 | −27.0 |
| 5 | 27 | 168 | 389 | 44 | 8.3 | −17.9 | −23.6 |
| 8 | 42 | 131 | 298 | 58 | 7.6 | −13.0 | −20.7 |
| 3 | 54 | 141 | 314 | 72 | 7.0 | −9.5 | −17.9 |
| 12 | 94 | 190 | 277 | 75 | 6.3 | −5.4 | −13.0 |
| 13 | 100 | 200 | 304 | 67 | 5.6 | −1.4 | −7.2 |
| 8 | 90 | 216 | 406 | 60 | 4.9 | 3.0 | −0.9 |
| 6 | 34 | 198 | 510 | 37 | 4.1 | 5.8 | 6.6 |
| 2 | 17 | 108 | 417 | 37 | 3.5 | 13.6 | 12.3 |
| 0 | 11 | 69 | 239 | 38 | 2.8 | 20.3 | 17.9 |
| 1 | 21 | 69 | 209 | 23 | 2.1 | 26.1 | 22.6 |
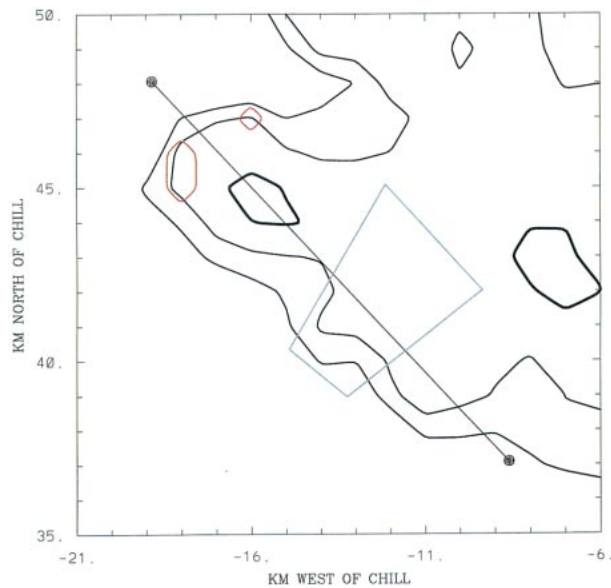
FIG. 9. CAPPI plot at 2151 UTC 28 Jul 1996. Analysis height is 6 km MSL. Black contours are reflectivity starting at 30 dBZ and increasing in 10-dB steps. 50-dBZ contour is darkened. Red contour is −25-dB LDR. Irregular gray box encloses the HDR hail signature that appeared at 2205 UTC. Line with solid dot endpoints locates the vertical cross section shown in Fig. 10.

that were applied in the 15 July 1998 case. The resultant CAPPI plot at the 6-km MSL height at 2151 is shown in Fig. 9. At this time, a small but expanding area of >50-dBZ echo was located in the right flank of the southeastward-moving storm ($X = -15.5$, $Y = 45$ km). LDR values of greater than −25 dB were found in only two small areas, both of which were outside of the 50-dBZ contour.

The corresponding vertical cross section through the right flank of the storm along the direction of echo motion is shown in Fig. 10. The reflectivity pattern in the cross-sectional plane showed the extensive vertical overhang structure typical of a vigorous convective cell. A column of reflectivities of greater than 50 dBZ reached heights of ~9.75 km MSL, but no significant areas of depolarization were present in the 50-dBZ core region at subfreezing temperatures. Significant LDR values were only found in the vicinity of the 0°C height where particle melting/freezing was likely to be taking place. No evidence of a positive $Z_{dr}$ column was present. Instead, the most prominent $Z_{dr}$ pattern was the downward depression in the $Z_{dr}$ contours across the low-altitude echo-core region where graupel melting was likely to be in progress (Bringi et al. 1986a).

The next analysis (2157) was based on the last volume scan in which no HDR hail signature was observed in the lowest sweep. Very rapid expansion of the area enclosed by the 50-dBZ reflectivity contour was evident at the 6-km height level (Fig. 11). The areal coverage of −25-dB LDR contour had also expanded considerably during the 7 min since the preceding CAPPI (Fig.

9). A substantial portion of this enhanced LDR area overlapped the 50-dBZ echo core at 2157.

These same evolutionary features were apparent in the 2157 vertical cross section (Fig. 12). Aloft, the 50-dBZ reflectivity contour had expanded and an area of reflectivities exceeding 60 dBZ had appeared near the −20°C height level. LDRs exceeding −25 dB had appeared in a volume that extended up to ~4 km above the environmental 0°C height. As was true at 2151, the 1-dB $Z_{dr}$ contour did not reach subfreezing heights.

Table 3 shows the sweep-by-sweep tabulations of the significant LDR gate occurrences for the two volumes discussed above. As in the 15 July 1998 case, a general increase in the number of significant LDR gates took place in the echo core in the 0° to −20°C temperature zone prior to the first appearance of the low-elevation-angle HDR hail signature (~2005). At lower heights where the temperatures were above 0°C, the percentage of significant LDR gates associated with reflectivities > 50 dBZ actually decreased between 2151 and 2158 UTC. As in the 15 July 1998 case, generalized precipitation particle melting tends to increase the LDR levels at these temperatures. For the purposes of this research, the LDR statistics at these above freezing temperatures are not taken to be meaningful until the HDR values indicate that hail has become a significant component of the near-surface precipitation.

The vertical cross sections show that positive $Z_{dr}$ column development was very different in the two analyzed events. These differences may have resulted from variations in the extent of neighboring echo. Cell development in the 1998 event took place within a large region of 30-dBZ echo whose base extended below the 0°C level (Fig. 6). Some of the particles responsible for this echo probably were composed of liquid–ice mixtures with varying ratios at heights below the 0°C level. Some of these particles, in turn, were likely to have been ingested into the intensifying updraft associated with the 0004 UTC hail onset. As noted in Conway and Zrnić (1993), the presence of these large particles in the updraft, some liquid and some only partially melted, would contribute to the formation of a well-defined positive $Z_{dr}$ column (as seen in the 1998 event). In contrast, the right flank development in the 1996 case took place in essentially echo-free surroundings, which may have limited the ingestion of large, preexisting particles into the updraft, thus reducing the prominence of the $Z_{dr}$ column.

In summary, polarimetric radar observations of the 15 July 1998 and the 28 July 1996 storms showed significant variability in development of a positive $Z_{dr}$ column. In both storms, the appearance of an HDR hail signature near the surface was preceded by an increase in LDRs in a portion of the parent storm's 50-dBZ echo volume at subfreezing temperatures. To understand better this LDR pattern evolution, the electromagnetic scattering behavior of growing hailstones was modeled.
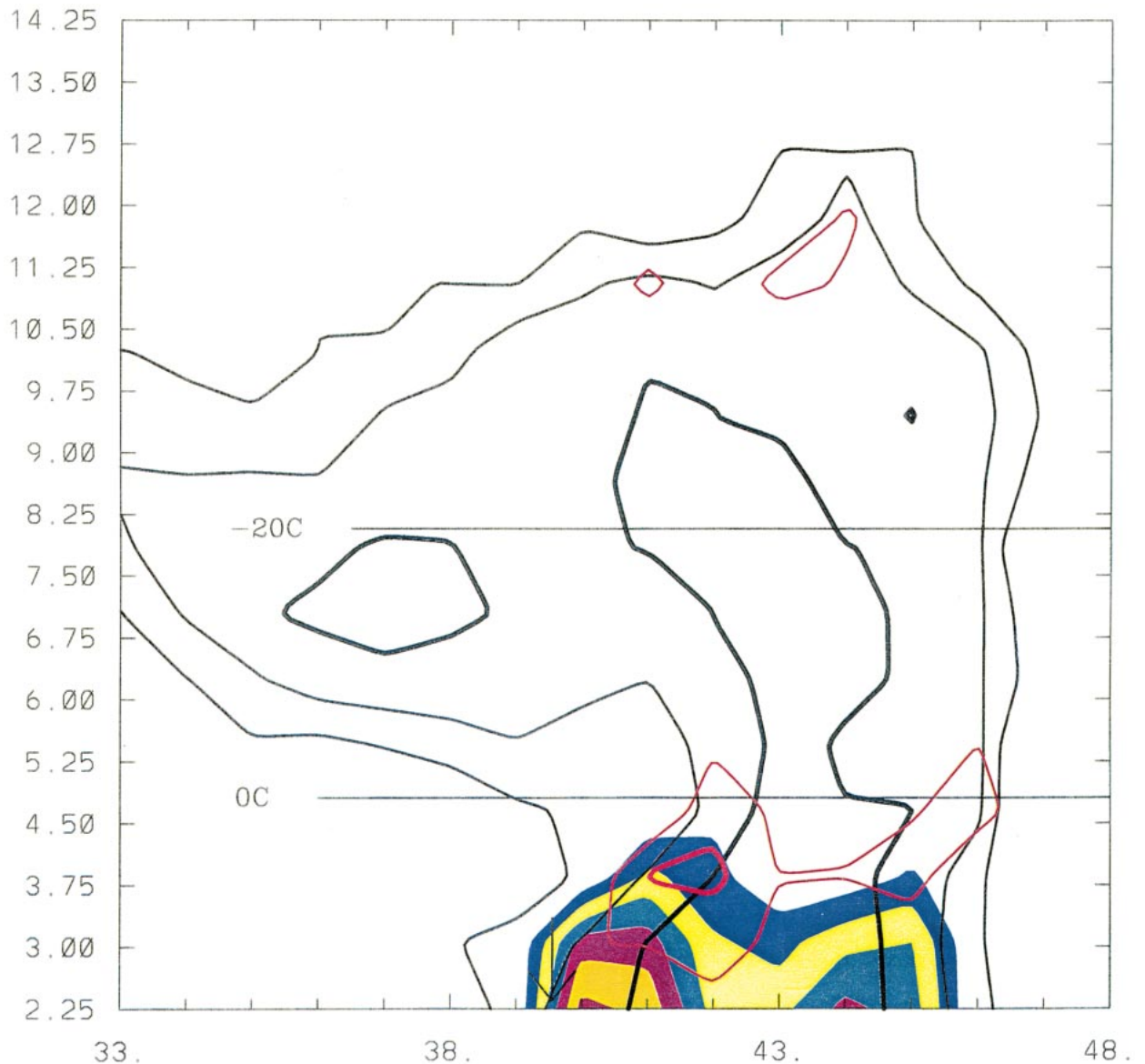
FIG. 10. Vertical cross section along 317° azimuth at 2151 UTC. Cross-section location is shown in Fig. 9. Black contours are reflectivity starting at 30 dBZ and increasing in 10-dB steps. 50-dBZ contour is darkened. The $Z_{dr}$s are color shaded starting at 1.0 dB, with an interval of 1.0 dB. Red LDR contours are −25 and −22 dB (−22-dB contour is darkened). Downward-pointing arrow near −36 km on the horizontal axis marks the location of the HDR hail signature at 2205 UTC.

## 4. Radar backscatter modeling

The electromagnetic backscatter properties of growing hailstones were simulated using a T-matrix-based scattering model (Waterman 1965; Seliga and Bringi; 1978). The fundamental input particle parameters are 1) the characteristic diameter and axis ratio, 2) a statistical representation of the particle's orientation (i.e., mean and standard deviation of the canting angle), and 3) the dielectric constant as defined by the particle's ice/water composition. The scattering model can process an input particle population with a specified size distribution (typically exponential). The net radar backscatter from

multiple particle types (i.e., mixed raindrops and hailstones) can also be calculated.

Although the model is capable of calculating the radar backscatter from a broad spectrum of particle specifications, it should be recognized that a number of fundamental simplifications from nature's true complexity need to be invoked. To make the solutions to the scattering equations mathematically tractable, spheroidal hailstone shapes were required. Various conical and irregular/lobed hailstone shapes were not considered. The ice particle's water component similarly was taken to be either uniformly distributed within the total hailstone
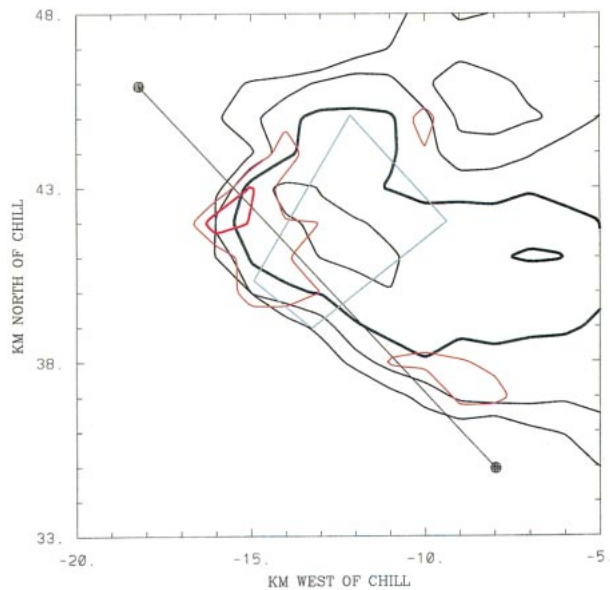
FIG. 11. As in Fig. 9 except analysis time is 2157 UTC. Red contours are −25- and −21-dB LDR; −21-dB contour is darkened.

from hailstones indicate the stones undergo large amplitude gyrations as they fall (Knight and Knight 1970). The water fraction in the hailstone ice structure was permitted to vary between 10% and 50%. This range generally includes the spectrum of values observed in artificial hailstones grown in a laboratory wind tunnel (Garcia-Garcia and List 1992). Consideration of the effect of hailstone water fraction is also warranted by the updraft liquid water content inferred in the primary case (15 July 1998). In this storm, the liquid water content in an adiabatic updraft was approximately 5 g kg$^{-1}$ at the −15°C level (390 hPa). The heat transfer studies reported by Bailey and Macklin (1968) suggest that the wet growth regime would be likely to occur for hailstones 1–2 cm in diameter under these temperature and liquid water content conditions.

Two different physical distributions of the hailstone's liquid water component were considered. Figure 13a shows the results when the liquid water was uniformly distributed within the hailstone [i.e., spongy or soaked conditions; Lesins and List (1986)]. The dielectric properties of the prescribed ice–water mixtures were calculated following the method of Bruggeman as summarized by Sihvola and Kong (1988). Over the modeled range of water fraction and canting angle standard deviation values, the LDR contours are essentially quasi-vertical lines. Significant (>−25 dB) LDR values are associated with water fractions greater than ∼27% (i.e., until the water fraction reaches ∼27%, none of the modeled canting angle standard deviations are capable of generating significant depolarizations).

The second hailstone water distribution simulates the case in which a combination of warm environmental temperature and high cloud liquid water content causes a water coating to exist on the stone's outer surface [wet growth; Lesins and List (1986)]. The modeled water coating thicknesses were calculated based on the same hailstone liquid water fractions shown in Fig. 13b. (The water mass implied by a given water fraction within a 1-cm major diameter, 0.8-axis-ratio hailstone was calculated. The equivalent water coating thickness was then determined by distributing this water mass uniformly over the hailstone's surface area.) Generally increased depolarization levels are produced when the hailstone water content is moved to the stone's outer surface (Fig. 13b vs Fig. 13a). The appreciable leftward shift of the −25-dB LDR contour between Figs. 13b and 13a demonstrates the LDR enhancement that even thin water coatings (∼0.3% to 0.5% of S-band wavelength) on hailstones are capable of generating significant values of LDR.

The implications of these calculations must be taken within the overall context of factors that influence LDR. As has been mentioned earlier, the scattering particle's shape and orientation are the primary geometric parameters that influence LDR. The final impact of these factors upon LDR is modulated by the particle's dielectric constant. Thus, contributions to the enhanced LDR val-

mass or else confined uniformly to the hailstone's surface. The effects of localized liquid water redistribution, shedding, and so on that have been observed in hailstones growing in laboratory wind tunnels (Garcia-Garcia and List 1992) had to be ignored.

Because no precipitation size spectra observations were available from the analyzed storms, the modeled scattering particles were taken to be a monodisperse population composed only of hailstones. Model test runs were done using 1) an exponential distribution of hailstone sizes and 2) the addition of a separate raindrop population with an exponential size distribution. In both cases, the calculated S-band LDR values were within 1 dB of those obtained from the simple monodisperse hail spectrum. A particle diameter of 1 cm was used as a general approximation of a growing hailstone. Based on the northeast Colorado hailstone collections tabulated by Knight (1986), a fixed axis ratio of 0.8 was assumed. In all of the results presented below, the particle temperature was prescribed to be 0°C. The calculations were carried out for a wavelength of 11 cm. The elevation angle was fixed at 5°.

The variable parameters in the T-matrix runs were the standard deviation of the mean hailstone canting angle and the liquid water characteristics of the scatterer's ice composition. The canting angle distribution was taken to be Gaussian about a mean canting angle of 0°. (The use of a random distribution of canting angles changed the modeled LDRs by approximately 0.7 dB from the results obtained using the Gaussian canting angle distribution.) For the simulations described here, the standard deviation of the hailstone canting angle was permitted to range from 30° to 60°, because examinations of the ice and air bubble patterns in thin sections cut
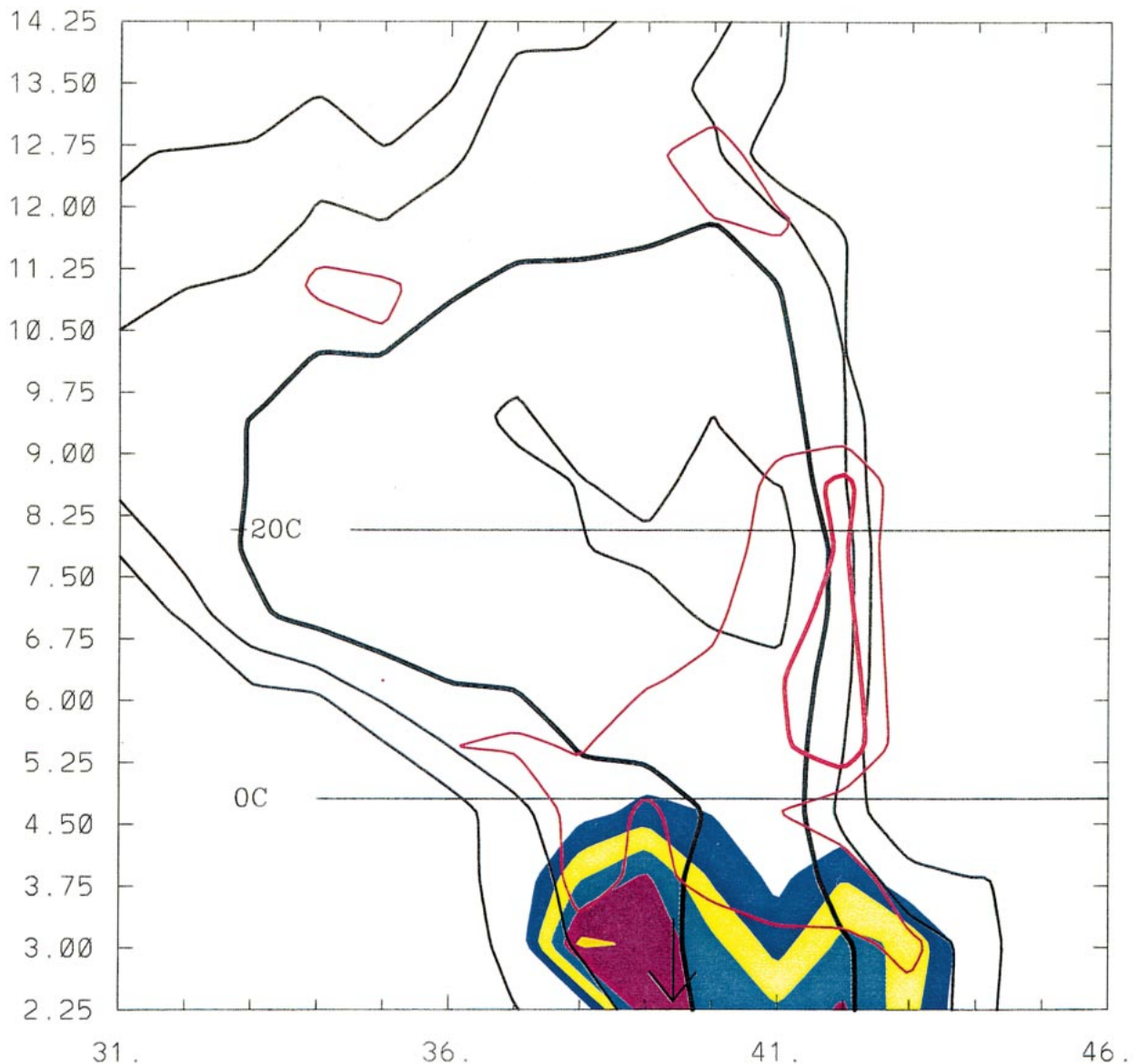
FIG. 12. As in Fig. 10, except plot time is 2157 UTC.

ues reported in this study might also have come from a combination of increasing axis ratios and/or large-amplitude gyratory motions within the population of developing hailstones. A qualitative appreciation for these factors can be obtained from additional considerations of the polarimetric radar measurements.

When the dispersion of particle axis ratios in the radar pulse volume increases (such that the number of particles with large axis ratios increases), the correlation between the H and V return signals adjusted to a time lag of zero [HV(0)] is decreased (Balakrishnan and Zrnić 1990). In both of our cases, the HV(0) values in the areas where enhanced LDRs developed aloft remained above ~0.90. In contrast, HV(0) values have been observed to drop to less than 0.80 in brightband

echoes where the combined presence of frozen, partially melted, and fully melted particles results in a very wide distribution of axis ratios (Illingworth and Caylor 1989). Thus, it does not appear that the existence of particles with unusually large of small axis ratios contributed significantly to the LDR enhancements observed in this study.

Outside of any positive $Z_{dr}$ column areas, the $Z_{dr}$ values were consistently near 0 dB in the inferred hail growth regions aloft. This near-0-dB $Z_{dr}$ condition did not display any organized spatial or temporal deviations; the hailstone orientations quickly became and remained widely dispersed throughout the growth process. There did not appear to have been an increase in canting angle fluctuations with time that was capable of producing the

TABLE 3. 28 Jul 1996 sweep-by-sweet counts of gates exceeding selected LDR values.

| LDR categories (dB) | | | | Percent of LDR > −25 dB within 50-dBZ echo | Avg height (km MSL) | Estimated moist adiabatic temperature (°C) | Avg sounding temperature (°C) |
|---|---|---|---|---|---|---|---|
| −19 | −21 | −23 | −25 | | | | |
| 2151:42 UTC volume | | | | | | | |
| 0 | 0 | 5 | 11 | 0 | 10.9 | −40.3 | −44.4 |
| 0 | 2 | 3 | 23 | 0 | 10.2 | −35.1 | −38.6 |
| 0 | 0 | 2 | 9 | 0 | 9.6 | −30.0 | −33.6 |
| 1 | 1 | 18 | 28 | 0 | 9.0 | −24.9 | −28.4 |
| 0 | 0 | 10 | 41 | 10 | 8.5 | −21.2 | −23.9 |
| 0 | 0 | 5 | 31 | 0 | 8.0 | −17.8 | −19.4 |
| 0 | 0 | 2 | 29 | 0 | 7.6 | −14.5 | −17.1 |
| 0 | 0 | 3 | 22 | 12 | 7.2 | −12.1 | −15.3 |
| 0 | 0 | 1 | 19 | 5 | 6.9 | −9.5 | −14.3 |
| 0 | 1 | 1 | 16 | 0 | 6.5 | −7.2 | −12.3 |
| 1 | 4 | 7 | 38 | 0 | 6.2 | −5.4 | −10.2 |
| 0 | 0 | 4 | 20 | 4 | 5.8 | −3.6 | −7.4 |
| 0 | 3 | 12 | 25 | 10 | 5.5 | −1.7 | −5.4 |
| 0 | 2 | 6 | 20 | 21 | 5.1 | 0.2 | −2.5 |
| 1 | 10 | 26 | 104 | 15 | 4.7 | 1.5 | 1.0 |
| 2 | 5 | 34 | 139 | 44 | 4.3 | 2.9 | 4.5 |
| 2 | 17 | 47 | 143 | 55 | 3.9 | 5.3 | 8.0 |
| 1 | 16 | 56 | 153 | 54 | 3.4 | 11.2 | 12.3 |
| 4 | 6 | 14 | 88 | 55 | 3.0 | 16.2 | 15.9 |
| 0 | 3 | 13 | 53 | 65 | 2.5 | 20.2 | 20.5 |
| 1 | 3 | 9 | 41 | 56 | 2.3 | 22.4 | 22.4 |
| 2 | 6 | 18 | 46 | 36 | 2.0 | 23.7 | 23.9 |
| 2158:06 UTC volume | | | | | | | |
| 0 | 0 | 0 | 0 | 0 | 13.2 | −61.2 | −61.3 |
| 0 | 0 | 0 | 2 | 0 | 12.5 | −56.5 | −56.3 |
| 0 | 0 | 0 | 11 | 0 | 11.8 | −49.6 | −52.5 |
| 0 | 0 | 5 | 22 | 4 | 11.1 | −42.7 | −46.2 |
| 1 | 4 | 16 | 76 | 9 | 10.4 | −36.6 | −40.3 |
| 0 | 2 | 11 | 48 | 13 | 9.7 | −30.8 | −34.5 |
| 1 | 2 | 12 | 46 | 26 | 9.1 | −26.2 | −29.3 |
| 0 | 1 | 16 | 58 | 21 | 8.6 | −22.1 | −24.8 |
| 0 | 1 | 10 | 52 | 48 | 8.1 | −18.5 | −20.3 |
| 0 | 1 | 15 | 52 | 34 | 7.7 | −15.4 | −17.7 |
| 0 | 2 | 11 | 47 | 67 | 7.3 | −12.8 | −15.6 |
| 0 | 5 | 17 | 42 | 55 | 6.9 | −9.9 | −14.3 |
| 2 | 5 | 25 | 94 | 46 | 6.6 | −7.7 | −13.0 |
| 0 | 2 | 20 | 91 | 51 | 6.2 | −5.9 | −10.2 |
| 4 | 8 | 29 | 92 | 62 | 5.9 | −4.0 | −8.1 |
| 2 | 5 | 32 | 67 | 59 | 5.6 | −2.1 | −6.1 |
| 8 | 11 | 44 | 89 | 54 | 5.2 | −0.2 | −3.4 |
| 1 | 7 | 37 | 121 | 45 | 4.8 | 1.1 | 0.1 |
| 6 | 9 | 36 | 153 | 37 | 4.4 | 2.5 | 3.6 |
| 0 | 10 | 43 | 217 | 39 | 4.1 | 3.6 | 6.2 |
| 5 | 13 | 55 | 196 | 47 | 3.7 | 7.2 | 9.7 |
| 1 | 11 | 32 | 177 | 46 | 3.3 | 12.6 | 13.2 |
| 1 | 4 | 21 | 95 | 35 | 2.9 | 16.8 | 16.9 |
| 1 | 0 | 13 | 48 | 29 | 2.5 | 20.7 | 20.5 |
| 2 | 2 | 26 | 70 | 14 | 2.2 | 22.6 | 22.9 |
| 0 | 2 | 17 | 72 | 12 | 2.0 | 23.9 | 23.9 |

generalized appearance of significantly high LDR levels.

In summary, the growing hail particles probably did not have axis ratios with extreme departures from unity. The canting angles of these particles underwent significantly large (several tens of degrees) excursions throughout their growth process. Within this overall growth regime, the hailstones' LDR characteristics were likely heavily influenced by the quantity and spatial distribution of water within the ice structure.

## 5. Discussion

The primary polarimetric radar evolutionary feature observed in this study was the noticeable increase in S-band LDR values exceeding −25 dB within the ~0° to
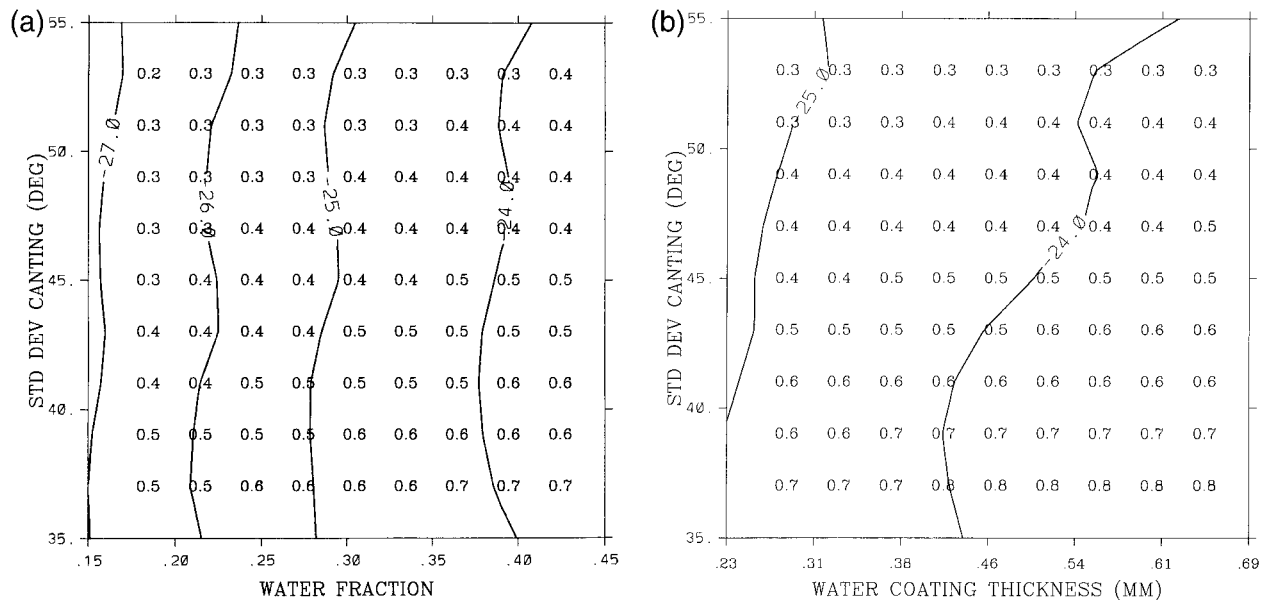
FIG. 13. (a) Selected hailstone backscattering properties obtained from a T-matrix model. Particle diameter is 1 cm, and aspect ratio (vertical dimension: horizontal dimension) is 0.8. Abscissa is the hailstone water fraction (%), ordinate is the std dev of the canting angle distribution (°). Contour lines are LDR values (dB); fractional values plotted at grid point locations are $Z_{dr}$s. (b) As in (a), except hailstone water component has been redistributed into a surface water coating. Abscissa is the water coating thickness (mm).

−20°C temperature levels in portions of nonsupercellular thunderstorm echo cores. These signatures occurred ~5–10 min before the appearance of near-surface hail. In particular, as surface hail became imminent, a noticeable increase in the number of gates containing > −25-dB LDRs took place within expanding areas of >50-dBZ echo aloft that flanked the preexisting storm core. This polarimetrically-inferred hail growth within an echo system's flanking region is in agreement with previous studies of multicell hailstorms (Heymsfield et al. 1980; Ziegler et al. 1983; Browning et al. 1976). Last, in only one of the analyzed storms (15 July 1998) was a positive $Z_{dr}$ column found to be associated with the elevated region of enhanced LDRs. As has been noted in other studies, the development of an "LDR cap" immediately downtrajectory from the summit of a positive $Z_{dr}$ column implies that vigorous hail growth process are likely to be under way (Conway and Zrnić 1993; Hubbert et al. 1998).

The available data do not permit the hail growth processes that were operative in these two cases to be analyzed in detail; such growth studies greatly benefit from accurate information on hail size spectra and on the incloud microphysical environment (Miller et al. 1990). However, the embryonic hailstones were likely to have been nonspherical frozen particles [i.e., millimeter-diameter frozen drops or graupel particles; Knight (1981)]. Because of their aerodynamic characteristics, such particles typically exhibit canting angle fluctuations on the order of several tens of degrees (Spengler and Gokhale 1972; List and Schemenaur 1971). These characteristics of asymmetric shape and gyrating motion

imply that the developing hailstones were capable of depolarizing the backscattered signal to significant levels. If these hailstones encounter vigorous growth conditions such that their bulk density increased, either through the development of a higher ice–air ratio, or through the accretion of unfrozen liquid water, the resultant dielectric constant change would further magnify the depolarized signal level. Because of the fundamental increase in sweep-out area with time for a growing hailstone, the mass accretion rate should tend to maximize in the later portion of the hail growth phase as the largest diameters are attained. If this accelerating mass accretion increased the hailstone density and/or water fraction, LDR enhancements would become increasingly likely during the later stages of the hail growth process.

The general hail-growth timescale implied by these radar observations is consistent with several numerical simulations of hail growth. Miller et al. (1990) reported that 15–20 min were required for ~1-mm-diameter embryos to grow into several centimeter–sized hailstones, with the majority of the stone mass being accreted during the descending (later) portion of the growth simulation. Ziegler et al. (1983) similarly integrated their hail growth model for 25 min to cover the entire embryo-to-hailstone growth process. Most of the growth to the maximum computed hail diameter in their simulations took place within a 10–15-min period. Last, Heymsfield et al. (1980) reported that in their computations, ~7 min of updraft residence time was required for a small hailstone to grow into a large hailstone (i.e., to increase in diameter from 1 to 1.5 cm). Taken together, these modeling studies suggest that the initial

appearance of enhanced S-band LDR values aloft is not likely to occur until the final $\sim$10 min of the hail growth process as the maximum diameters are attained.

This short timescale clearly limits the utility of using the initial development of enhanced LDR areas aloft to issue anticipatory hail warnings. Based on this study, a time window of only $\sim$10 min exists between the initial detection of an elevated volume of significantly depolarized core echo aloft and the appearance of significant hail at the surface. When the radar volume scan time resolution is on the order of 6 min, the pattern of LDR enhancement will appear suddenly, generally no more than two volume scans before the onset of the hail event at the surface. However, it should be noted that, in both of the storms examined here, the initial appearance of an enhanced LDR region aloft quickly evolved into a columnar region of enhanced LDR that extended from the surface to altitudes that were several kilometers above the 0°C height. This column then persisted as long as the storm was producing a significant hail swath. Thus, in addition to whatever hail prediction capabilities that LDR observations may possess, it may also be useful as a diagnostic parameter for thunderstorm hail production.

Furthermore, the analysis of additional storms during the course of this research revealed that not all near-surface high $Z_{HH}$–low $Z_{dr}$ patterns were preceded by organized areas of LDR enhancement aloft. However, the surface hail reported in these null cases was consistently of small, nondamaging sizes. Thus, the detection of organized regions of enhanced LDRs within portions of thunderstorm echo cores aloft may identify the storms that are the most likely to produce damaging hail.

The implications of this study's results should also be examined under a broader range of environmental conditions. For example, convective cloud bases are likely to be warmer and more moist in storms developing outside of the U.S. high plains environment. Existing research has shown that positive $Z_{dr}$ columns are commonly observed when vigorous convective growth takes place in a moist environment (Bringi et al. 1997). The implied greater updraft moisture content would also have several important effects on the evolution of the LDR field. The enhanced precipitation formation by coalescence would increase the likelihood that drops large enough to have an appreciable freezing time would be available for lofting above the 0°C level. Depolarization levels would then be enhanced during the subsequent drop freezing process (Smith et al. 1999; Bringi et al. 1997). Increased updraft moisture content might also be expected to promote an increased water fraction in the growing, frozen hydrometeors, thus tending to increase the depolarization levels. However, at lower elevations in these more tropical environments, melting would play a greater role in reducing the diameters of the hailstones during their final descent. In the limit, such melting could cause precipitation grown in a significantly depolarized echo core aloft to reach the sur-

face only as rain. Also, none of the storms analyzed here showed marked steady-state characteristics. It is quite possible that the patterns by which hail grows aloft and subsequently descends to the ground in storms with more supercellular organization will vary from those seen in this study. Thus, it would be useful to collect polarimetric radar observations of convective storms with various organizational modes in a variety of climatic areas.

## REFERENCES

Atlas, D., and F. H. Ludlam, 1961: Multiple-wavelength radar reflectivity of hailstorms. *Quart. J. Roy. Meteor. Soc.,* **87,** 523–534.

——, M. Kerker, and W. Hitschfeld, 1953: Scattering and attenuation by non-spherical atmospheric particles. *J. Atmos. Terr. Phys.,* **2,** 108–119.

Aydin, K., T. A. Seliga, and V. Balaji, 1986: Remote sensing of hail with a dual linear polarization radar. *J. Climate Appl. Meteor.,* **25,** 1475–1484.

Bailey, I. H., and W. C. Macklin, 1968: Heat transfer from artificial hailstones. *Quart. J. Roy. Meteor. Soc.,* **94,** 93–98.

Balakrishnan, N., and D. S. Zrnić, 1990: Use of polarization to characterize precipitation and discriminate large hail. *J. Atmos. Sci.,* **47,** 1525–1540.

Barge, B. L., 1970: Polarization observations in Alberta. Preprints, *14th Radar Meteorology Conf.,* Tucson, AZ, Amer. Meteor. Soc., 221–224.

Bringi, V. N., R. M. Rasmussen, and J. Vivekanandan, 1986a: Multiparameter radar measurements in Colorado convective storms. Part I: Graupel melting studies. *J. Atmos. Sci.,* **43,** 2545–2563.

——, J. Vivekanandan, and J. D. Tuttle, 1986b: Multiparameter radar measurements in Colorado convective storms. Part II: Hail detection studies. *J. Atmos. Sci.,* **43,** 2564–2577.

——, K. Knupp, A. Detwiler, L. Liu, I. J. Caylor, and R. A. Black, 1997: Evolution of a Florida thunderstorm during the Convection and Precipitation/Electrification experiment: The case of 9 August 1991. *Mon. Wea. Rev.,* **125,** 2131–2160.

Browning, K. A., and G. B. Foote, 1976: Airflow and hail growth in supercell storms and some implications for hail suppression. *Quart. J. Roy. Meteor. Soc.,* **102,** 499–533.

——, and Coauthors, 1976: Structure of an evolving hailstorm. Part V: Synthesis and implications for hail growth and hail suppression. *Mon. Wea. Rev.,* **104,** 603–610.

Brunkow, D. A., V. N. Bringi, P. C. Kennedy, S. A. Rutledge, V. Chandrasekar, E. A. Mueller, and R. K. Bowie, 2000: A description of the CSU–CHILL national radar facility. *J. Atmos. Oceanic Technol.,* **17,** 1596–1608.

Conway, J. W., and D. S. Zrnić, 1993: A study of embryo production

and hail growth using dual-Doppler and multiparameter radars. *Mon. Wea. Rev.,* **121,** 2511–2528.

Cressman, G. P., 1959: An operative objective analysis scheme. *Mon. Wea. Rev.,* **87,** 367–374.

Donaldson, R. J., 1961: Radar reflectivity profiles in thunderstorms. *J. Meteor.,* **18,** 292–305.

Garcia-Garcia, F., and R. List, 1992: Laboratory measurements and parameterizations of supercooled water skin temperatures and bulk properties of gyrating hailstones. *J. Atmos. Sci.,* **49,** 2058–2073.

Herzegh, P. H., and A. R. Jameson, 1992: Observing precipitation through dual-polarization radar measurements. *Bull. Amer. Meteor. Soc.,* **73,** 1365–1374.

Heymsfield, A. J., A. R. Jameson, and H. W. Frank, 1980: Hail growth mechanisms in a Colorado storm: Hail formation processes. *J. Atmos. Sci.,* **37,** 1779–1807.

Holler, H., V. N. Bringi, J. Hubbert, M. Hagen, and P. F. Meischner, 1994: Life cycle and precipitation formation in a hybrid-type hailstorm revealed by polarimetric and Doppler radar measurements. *J. Atmos. Sci.,* **51,** 2500–2522.

Hubbert, J. C., V. N. Bringi, L. D. Carey, and S. Bolen, 1998: CSU–CHILL polarimeteric radar measurements in a severe hailstorm in eastern Colorado. *J. Appl. Meteor.,* **37,** 748–775.

Humphries, R. G., 1974: Observations and calculations of depolarization effects at 3 GHz due to precipitation. *J. Rech. Atmos.,* **8,** 155–161.

Illingworth, A. J., and I. J. Caylor, 1989: Cross polar observations of the bright band. Preprints, *24th Conf. on Radar Meteorology,* Tallahassee, FL, Amer. Meteor. Soc., 323–327.

——, J. W. F. Goddard, and S. M. Cherry, 1987: Polarization radar studies of precipitation development in convective storms. *Quart. J. Roy. Meteor. Soc.,* **113,** 469–489.

Jameson, A. R, 1983: Microphysical interpretation of multi-parameter radar measurements in rain. Part II: Estimation of raindrop size distribution parameters by combined dual-wavelength and polarization measurements. *J. Atmos. Sci.,* **40,** 1803–1813.

——, M. J. Murphy, and E. P. Krider, 1996: Multiple-parameter radar observations of isolated Florida thunderstorms during the onset of electrification. *J. Appl. Meteor.,* **35,** 343–354.

Johnson, D. B., 1987: On the relative efficiency of coalescence and riming. *J. Atmos. Sci.,* **44,** 1671–1680.

Knight, C. A., and N. C. Knight, 1970: The falling behavior of hailstones. *J. Atmos. Sci.,* **27,** 672–681.

Knight, N. C., 1981: The climatology of hailstone embryos. *J. Appl. Meteor.,* **20,** 750–755.

——, 1986: Hailstone shape factor and its relationship to radar interpretation of hail. *J. Climate Appl. Meteor.,* **25,** 1956–1958.

Lesins, G. B., and R. List, 1986: Sponginess and drop shedding of gyrating hailstones in a pressure-controlled icing wind tunnel. *J. Atmos. Sci.,* **43,** 2813–2825.

List, R., and R. Schemenauer, 1971: Free-fall behavior of planar snow crystals, conical graupel, and small hail. *J. Atmos. Sci.,* **28,** 110–115.

Ludlam, F. H., 1980: *Clouds and Storms: The Behavior and Effect of Water in the Atmosphere.* The Pennsylvania State University Press, 405 pp.

McCormick, G. C., and A. Hendry, 1975: Principles for the radar determination of the polarization properties of precipitation. *Radio Sci.,* **10,** 421–434.

Miller, L. J., J. D. Tuttle, and G. B. Foote, 1990: Precipitation production in a large Montana thunderstorm: Airflow and particle growth trajectories. *J. Atmos. Sci.,* **47,** 1619–1646.

Mohr, C. G., and L. J. Miller, 1983: CEDRIC—a software package for Cartesian space editing, synthesis, and display of radar data fields under interactive control. Preprints, *21st Conf. on Radar Meteorology,* Edmonton, AB, Canada, Amer. Meteor. Soc., 569–574.

NCDC, 1996: *Storm Data.* Vol. 38, No. 7, 363 pp.

Oye, R., and R. Carbone, 1981: Interactive Doppler editing software. Preprints, *20th Conf. on Radar Meteorology,* Boston, MA, Amer. Meteor. Soc., 683–689.

Pruppacher, H. R., and K. V. Beard, 1970: A wind tunnel investigation of the internal circulation and shape of water drops falling at terminal velocity in air. *Quart. J. Roy. Meteor. Soc.,* **96,** 247–256.

Rinehart, R. E., and J. D. Tuttle, 1982: Antenna beam patterns and dual wavelength processing. *J. Appl. Meteor.,* **21,** 1865–1880.

Seliga, T. A., and V. N. Bringi, 1976: Potential use of radar differential reflectivity measurements at orthogonal polarizations for measuring precipitation. *J. Appl. Meteor.,* **15,** 69–76.

——, and ——, 1978: Differential reflectivity and differential phase shift: Applications in radar meteorology. *Radio Sci.,* **13,** 271–275.

Sihvola, A. H., and J. A. Kong, 1988: Effective permittivity of dielectric mixtures. *IEEE Trans. Geosci. Remote Sens.,* **26,** 420–429.

Smith, P. L., D. J. Musil, A. G. Detwiler, and R. Ramachandran, 1999: Observations of mixed-phase precipitation within a CaPE thunderstorm. *J. Appl. Meteor.,* **38,** 145–155.

Spengler, J. D., and N. Gokhale, 1972: Freezing of freely suspended, supercooled water drops in a large vertical wind tunnel. *J. Appl. Meteor.,* **11,** 1101–1107.

Tuttle, J. D., and R. E. Rinehart, 1983: Attenuation correction in dual-wavelength analyses. *J. Climate Appl. Meteor.,* **22,** 1914–1921.

——, V. N. Bringi, H. D. Orville, and F. J. Kopp, 1989: Multiparameter radar study of a microburst: Comparison with model results. *J. Atmos. Sci.,* **46,** 601–620.

Waterman, P. C., 1965: Matrix formulation of electromagnetic scattering. *Proc. IEEE,* **53,** 805–812.

Ziegler, C. L., P. S. Ray, and N. C. Knight, 1983: Hail growth in an Oklahoma multicell storm. *J. Atmos. Sci.,* **40,** 1768–1791.